

Hidden Higgs Portal Vector Dark Matter for the Galactic Center Gamma-Ray Excess from the Two-Step Cascade Annihilation, and Muon $g - 2$

Kwei-Chou Yang^{1,*}

¹*Department of Physics and Center for High Energy Physics,
Chung Yuan Christian University, Taoyuan 320, Taiwan*

We have built a lepton-specific next-to-minimal two-Higgs-doublet-portal vector dark matter model. The vector dark matter in the hidden sector does not directly couple to the visible sector, but instead annihilates into the hidden Higgs bosons which decay through a small coupling into the CP-odd Higgs bosons. In this model, the Galactic center gamma-ray excess is mainly due to the 2-step cascade annihilation with τ 's in the final state. The obtained mass of the CP-odd Higgs A in the Galactic center excess fit can explain the muon $g - 2$ anomaly at the 2σ level without violating the stringent constraints from the lepton universality and τ decays. We show three different freeze-out types of the dark matter relic, called (i) the conventional WIMP dark matter, (ii) the unconventional WIMP dark matter and (iii) the cannibally co-decaying dark matter, depending on the magnitudes of the mixing angles between the hidden Higgs and visible two-Higgs doublets. The dark matter in the hidden sector is secluded from detections in the direct searches or colliders, while the dark matter annihilation signals are not suppressed in a general hidden sector dark matter model. We discuss the constraints from observations of the dwarf spheroidal galaxies and the Fermi-LAT projected sensitivity.

arXiv:1806.05663v2 [hep-ph] 30 Jul 2018

* kcyang@cycu.edu.tw

I. INTRODUCTION

The evidence for the dark matter (DM) in the Universe has been well established from various astronomical observations and cosmological measurements. The DM, which cannot be accounted for within the standard model (SM) scenario, indicates the existence of new physics. The attractive candidates for the DM are the so-called weakly interacting massive particles (WIMPs) which, having a weak scale mass and annihilating into SM particles via weak scale couplings, can provide a correct thermal relic abundance, following the Boltzmann suppression before freeze-out.

Several collaborations have reported an excess of GeV gamma-rays near the region of the Galactic center (GC) [1–11], where the excess spectrum can be fitted using DM annihilation models. Although the excess result might be explained by the millisecond pulsars or some other astrophysical sources [12–18], the DM annihilation is a viable scenario from the particle physics point of view [19–35]. However, the DM models capable of explaining the GC gamma-ray excess are increasingly constrained by direct detection experiments and measurements at colliders. Some ideas have been proposed that can avoid overproduced signals in the latter two experiments; for instance, the DM annihilates into $b\bar{b}$ through a pseudoscalar mediator exchange [19–21, 35]. The present work is motivated by the idea called “secluded WIMP dark matter” in which the DM first annihilates to a pair of short-lived hidden mediators which subsequently decay into SM particles through very small couplings [29–40], so that it can easily evade the stringent constraints from current measurements, but provide observable gamma-ray signals in the indirect measurements.

In this paper, we will use the GC gamma-ray excess spectrum obtained by Calore, Cholis and Weniger (CCW) who analyzed the Fermi data in a consistent treatment of systematic uncertainties that came from the modeling of the Galactic diffuse emission background [8]. It is interesting to note that if the dark matter annihilates directly only into the $\tau^+\tau^-$, the spectral fit to the GC gamma-ray GeV excess gives the best-fit result with dark matter mass ~ 9.5 GeV, and low-velocity annihilation cross section $\langle\sigma v\rangle \simeq 0.37 \times 10^{-26}$ cm³s⁻¹, nevertheless corresponding to a lower p -value ~ 0.05 for the goodness-of-fit test [8]. The direct DM annihilation to $\tau^+\tau^-$ produces a gamma-ray spectrum which peaks sharply at a little higher energies. If the annihilation processes present some extra intermediate steps, the final state τ 's generated from the cascade decays are boosted, and therefore the resultant gamma-ray spectrum becomes broader and has a better fit to the GC excess observation [41, 42]. We are interested in the two-step cascade annihilation process (see Fig. 1 for reference). The reason is that not only a much larger p -value ~ 0.22 can be obtained, but also the fitted DM mass and annihilation cross section are enlarged by a factor

of ~ 4 , compared with the direct annihilation to $\tau^+\tau^-$. The resulting annihilation cross section required to explain the GC excess signals is thus in good agreement with that required by the correct relic abundance in the thermal WIMP scenario.

Here, we make an extension for the "secluded DM" idea. We will build a hidden sector dark matter model in which the produced gamma-ray spectrum is mostly generated by the final state, τ 's, resulted from the two-step cascade annihilation of the vector dark matter. After spontaneous symmetry breaking, the hidden dark sector maintaining the dark discrete Z_2 symmetry is composed of a singlet vector boson (the dark matter) and a real hidden Higgs (the mediator), where the latter will mix with the 2 neutral CP-even Higgs bosons of the lepton-specific two-Higgs-doublet model (2HDM) which is also called the type-X 2HDM. Moreover, in the two Higgs doublets the two extra neutral Higgs bosons, one CP-even and one CP-odd, couple to leptons are enhanced in large $\tan\beta$ limit, whereas their couplings to quarks are suppressed. The main mechanism in this model for describing the GC excess is that the DM annihilation to the mediator pair is followed by the mediator decays to CP-odd Higgs bosons, A , which subsequently decay into taus. We find that the resultant masses for DM and CP-odd Higgs are $m_X \sim 25 - 50$ GeV and $m_A \sim 3.6 - 25$ GeV, respectively. Our result for m_A , in a good agreement with the allowed range given in the type-X 2HDM [43–45], can accommodate the muon $g - 2$ anomaly at 2σ level, under the constraints from the lepton universality and τ decays.

In the present case, the CP-odd boson A is in chemical and thermal equilibrium with the SM thermal bath before the DM freeze out. However, the dependence of the DM freeze-out temperature and corresponding thermally averaged annihilation cross section on the mixing angles of the hidden Higgs and 2HDM is subtle. At a temperature below the mass of the mediator S , the chemical equilibrium of S with the thermal bath is maintained mainly through $S \leftrightarrow AA$. If the mixing angles are not too small, the hidden Higgs mediator can be in thermal equilibrium with the bath, such that the DM particles behave like WIMPs, which exhibit the Boltzmann suppression until the freeze-out temperature.

However, due to small mixing angles, resulting in that the coupling constant of the mediator to the A boson is too small to ensure the required decay width of the S boson to keep the dark sector in chemical equilibrium with the bath, the dark sector will decouple from the thermal background at the temperature below the mediator's mass. If so, the comoving number density of the dark sector will not exponentially deplete until the occurrence of the mediator decaying to the A pair. Such the mechanism was discussed by Dror, Kuflik, and Ng [46] and by Farina, Pappadopulo, Ruderman, and Trevisan [47], where the former used a degenerate hidden sector to illustrate the

idea for the DM, called ‘‘co-decaying dark matter’’. Our case is more relevant to the non-degenerate one, for which the hidden mediator undergoes cannibalism first [47, 48] and, after that phase, the exponential suppression for comoving dark matter number density could occur much earlier than that for the mediator due to a significantly suppressed up-scattering rate for the process. More detailed discussions will be presented in Sec. VB.

This paper is organized as follows. In Sec. II, we describe the model. The relevant ingredients, including the Yukawa sectors, Higgs couplings, and the decay widths of the mediator and CP-odd Higgs boson are presented. In Sec. III, we discuss the experimental and theoretical constraints on parameters related to the two-Higgs doublets and Yukawa sectors. In Sec. IV, we first outline the approach of determining the gamma-ray spectrum from a 2-step cascade annihilation to the final state τ ’s, and then describe the analysis and results concerning gamma-ray observations, compared with the relic abundance in the conventional WIMP dark matter scenario. Sec. V contains the analysis for the mixing angles between the hidden scalar and two neutron CP-even bosons in the two Higgs doublets. The discussions and conclusions are given in Sec. VI.

II. LEPTON-SPECIFIC NEXT-TO-MINIMAL 2HDM PORTAL VECTOR DARK MATTER

A. The Model

We consider a model with two Higgs doublets, Φ_1, Φ_2 , and a complex scalar dark Higgs field Φ_S . The CP-conserving potential for the Higgs sector is described by

$$\begin{aligned}
 V = & m_{11}^2 |\Phi_1|^2 + m_{22}^2 |\Phi_2|^2 - m_{12}^2 (\Phi_1^\dagger \Phi_2 + h.c.) + \frac{\lambda_1}{2} (\Phi_1^\dagger \Phi_1)^2 + \frac{\lambda_2}{2} (\Phi_2^\dagger \Phi_2)^2 \\
 & + \lambda_3 (\Phi_1^\dagger \Phi_1) (\Phi_2^\dagger \Phi_2) + \lambda_4 (\Phi_1^\dagger \Phi_2) (\Phi_2^\dagger \Phi_1) + \frac{\lambda_5}{2} [(\Phi_1^\dagger \Phi_2)^2 + h.c.] \\
 & + m_{33}^2 \Phi_S^\dagger \Phi_S + \frac{\lambda_6}{2} (\Phi_S^\dagger \Phi_S)^2 + \lambda_7 (\Phi_1^\dagger \Phi_1) (\Phi_S^\dagger \Phi_S) + \lambda_8 (\Phi_2^\dagger \Phi_2) (\Phi_S^\dagger \Phi_S), \quad (1)
 \end{aligned}$$

where Φ_S is a singlet under the SM gauge fields. As usual, we have imposed a discrete \mathbb{Z}_2 symmetry to the Higgs potential, such that $\Phi_1 \rightarrow \Phi_1$, $\Phi_2 \rightarrow -\Phi_2$, and $\Phi_S \rightarrow \Phi_S$, under which the tree-level flavor changing neutral currents (FCNCs) are absent. The \mathbb{Z}_2 symmetry is softly broken by the term containing m_{12}^2 . On the other hand, we have considered that Φ_S is charged in the dark $U_{\text{dm}}(1)$ gauge group, while other Higgs fields and SM particles have no such quantum number. The $U_{\text{dm}}(1)$ group contains an abelian gauge boson, X_μ . After spontaneous symmetry breaking, the vacuum expectation value (VEV) of Φ_S generates a mass for X_μ , and a discrete \mathbb{Z}'_2 symmetry:

$X_\mu \rightarrow -X_\mu, \Phi_S \rightarrow \Phi_S^*$, is still maintained, such that X_μ is stable and can serve as a (vector) dark matter candidate.

The relevant kinetic terms in the dark sector are given by

$$\mathcal{L}_{\text{DM}} = -\frac{1}{4}X_{\mu\nu}X^{\mu\nu} + (D_\mu\Phi_S)^\dagger(D^\mu\Phi_S), \quad (2)$$

where $X_{\mu\nu} = \partial_\mu X_\nu - \partial_\nu X_\mu$, and the covariant derivative is defined as

$$D_\mu\Phi_S = (\partial_\mu + ig_X Q_{\Phi_S} X_\mu)\Phi_S, \quad (3)$$

with Q_{Φ_S} the $U_{\text{dm}}(1)$ charge of Φ_S . After spontaneous symmetry breaking, we have

$$\Phi_S = \frac{1}{\sqrt{2}}(v_S + h_3), \quad (4)$$

where the imaginary part of Φ_S is absorbed by the vector gauge boson (dark matter) due to the \mathbb{Z}'_2 symmetry: $X_\mu \rightarrow -X_\mu$, and the vector gauge boson obtains a mass, $m_X = g_X Q_{\Phi_S} v_S$ (see also Refs. [23–27, 49, 50] for related discussions). In this paper, we will simply take $Q_{\Phi_S} = 1$; in other words, Q_{Φ_S} and g_X are lumped together. The interacting terms of the dark sector is given by

$$\mathcal{L}_{\text{DM}}^{\text{int}} \supset \frac{1}{2}g_X^2 X_\mu X^\mu h_3^2 + g_X m_X X_\mu X^\mu h_3, \quad (5)$$

where the hidden scalar field h_3 will mix with the neutral scalars in the two Higgs doublets through the interaction given by Eq. (1).

After spontaneous symmetry breaking, the version of the Higgs sector becomes the next-to-minimal two-Higgs-doublet model (N2HDM). We decompose the Higgs doublet fields as

$$\Phi_i = \begin{pmatrix} h_i^+ \\ \frac{1}{\sqrt{2}}(v_i + h_i + ia_i) \end{pmatrix}, \quad \text{with } i = 1, 2, \quad (6)$$

where the vacuum expectation values (VEVs) of the doublets approximately satisfy $v_1^2 + v_2^2 \approx v^2 = (246 \text{ GeV})^2$, with v being the SM VEV. The scalar fields in Φ_i and Φ_S can be expressed in terms of mass eigenstates of physical Higgs states and Goldstone bosons as

$$\begin{pmatrix} h_1^\pm \\ h_2^\pm \end{pmatrix} = \begin{pmatrix} \cos\beta & -\sin\beta \\ \sin\beta & \cos\beta \end{pmatrix} \begin{pmatrix} G^\pm \\ H^\pm \end{pmatrix}, \quad (7)$$

$$\begin{pmatrix} a_1 \\ a_2 \end{pmatrix} = \begin{pmatrix} \cos\beta & -\sin\beta \\ \sin\beta & \cos\beta \end{pmatrix} \begin{pmatrix} G^0 \\ A \end{pmatrix}, \quad (8)$$

$$\begin{pmatrix} h_1 \\ h_2 \\ h_3 \end{pmatrix} = \begin{pmatrix} \cos\alpha & -\sin\alpha & 0 \\ \sin\alpha & \cos\alpha & 0 \\ 0 & 0 & 1 \end{pmatrix} \begin{pmatrix} 1 & 0 & 0 \\ 0 & \cos\delta & -\sin\delta \\ 0 & \sin\delta & \cos\delta \end{pmatrix} \begin{pmatrix} \cos\theta & 0 & -\sin\theta \\ 0 & 1 & 0 \\ \sin\theta & 0 & \cos\theta \end{pmatrix} \begin{pmatrix} H \\ h \\ S \end{pmatrix}, \quad (9)$$

where (H, h) are the (heavy, light) Higgs CP-even scalars in the two Higgs doublets in the limit of $\delta, \theta \rightarrow 0$, A the CP-odd scalar, H^\pm the two charged Higgs bosons, and (G^\pm, G^0) the Goldstone bosons corresponding to the longitudinal components of W^\pm and Z , respectively. Here β is the mixing angle of the charged bosons, and α is the mixing angle of neutral CP-even bosons (h_1, h_2) in the limit of $\delta, \theta \rightarrow 0$, where the former is defined as $\tan \beta = v_2/v_1$.

The theoretical requirements for the perturbativity, vacuum stability, and tree-level perturbative unitarity are given in Appendix A. From the results for the square of masses of H^\pm and A , square of mass matrix of H, h and S , and the minimum conditions of the Higgs potential at the VEV, the quartic couplings λ_i , with $i \equiv 1, \dots, 8$, can be rewritten in terms of the $m_h^2, m_H^2, m_A^2, m_{H^\pm}^2$ and $M^2[\equiv m_{12}^2/(s_\beta c_\beta)]$. We show the relations in Appendix B.

B. The Yukawa Sectors

The type-X Yukawa interactions are imposed a Z_2 symmetry only to the right-handed quarks, $u_R \rightarrow -u_R$ and $d_R \rightarrow -d_R$. Thus, the Yukawa Lagrangian, describing the interactions of the Higgs doublets to the SM fermions, is given by

$$\mathcal{L}_{\text{Yukawa}} = -\bar{Q}_L y_u \tilde{\Phi}_2 u_R - \bar{Q}_L y_d \Phi_2 d_R - \bar{L}_L y_\ell \Phi_1 \ell_R + h.c., \quad (10)$$

where $\tilde{\Phi}_2 = i\sigma_2 \Phi_2^*$, and y_i is the 3×3 Yukawa matrix. In terms of the mass eigenstates of the scalar bosons, the Yukawa interaction terms can be rewritten by

$$\begin{aligned} \mathcal{L}_{\text{Yukawa}} \supset & - \sum_{f=u,d,\ell} \frac{m_f}{v} \left(\frac{\bar{\xi}_f}{c_\beta} h_f \bar{f} f - i \text{sgn}(f) \xi_f A \bar{f} \gamma_5 f \right) \\ & + \left[\sqrt{2} V_{ud} H^+ \bar{u} \left(\frac{m_u \xi_u}{v} P_L - \frac{m_d \xi_d}{v} P_R \right) d - \frac{\sqrt{2} m_\ell \xi_\ell}{v} H^+ \bar{\nu} P_R \ell + h.c. \right], \quad (11) \end{aligned}$$

where $h_{u,d} \equiv h_2$, $h_\ell \equiv h_1$, $\bar{\xi}_{u,d} = \xi_{u,d} = \cot \beta$, $\bar{\xi}_\ell = 1$, $\xi_\ell \equiv -\tan \beta$, $P_R = (1 + \gamma_5)/2$, $P_L = (1 - \gamma_5)/2$ and V_{ud} is the Cabibbo-Kobayashi-Maskawa matrix element. Keeping small terms linear in $\sin \theta$ and $\sin \delta$, the Yukawa couplings of the neutral Higgs bosons in the type-X N2HDM, normalized with respect to the SM Higgs, are given in Table I, where $g_{Aff} \equiv \text{sgn}(f) \xi_f$.

For the type-X Yukawa interactions, the normalized lepton Yukawa coupling to the SM Higgs is given by

$$g_{h\ell\ell} = -\frac{s_\alpha}{c_\beta} = s_{\beta-\alpha} - t_\beta c_{\beta-\alpha}. \quad (12)$$

Considering the LHC data but without muon $g - 2$ constraint, the allowed parameters, consistent with the alignment limit of $s_{\beta-\alpha} \rightarrow 1$, lie in two different regions [43]; in one region, the $g_{h\ell\ell}$

	$f = u, d$	$f = \ell$
g_{hff}	c_α/s_β	$-s_\alpha/c_\beta$
g_{Hff}	s_α/s_β	c_α/c_β
g_{Sff}	$-(s_\alpha s_\theta + c_\alpha s_\delta)/s_\beta$	$(-c_\alpha s_\theta + s_\alpha s_\delta)/c_\beta$
g_{Aff}	$\pm 1/t_\beta$	t_β

TABLE I. The tree level Yukawa couplings of the neutral type-X N2HDM Higgs bosons, keeping terms linear in $\sin \theta$ and $\sin \delta$, with respect to that of the SM Higgs.

couplings ($\rightarrow 1$) have values near the SM ones, while in the other region which is called the wrong-sign region, the $g_{h\ell\ell} \rightarrow -1$ has opposite sign to the SM Higgs couplings to VV , (normalized) $g_{hVV,hZZ} = s_{\beta-\alpha} \rightarrow 1$, and to the quark pair, $g_{hff} = c_\alpha/s_\beta = s_{\beta-\alpha} + c_{\beta-\alpha}/t_\beta \rightarrow 1$ for a large $\tan \beta$ satisfying $2t_\beta c_{\beta-\alpha} \sim 2$. Only the wrong-sign region is favored by the muon $g-2$ measurement [43] (see also the following discussion in this work).

On the other hand, for the type-X Yukawa interactions, the couplings, $g_{A\ell\ell}$ and $g_{H\ell\ell} \propto \tan \beta$, are enhanced by a large $\tan \beta$, while g_{Aqq} and $g_{Hqq} \propto 1/\tan \beta$ are suppressed, where $q \equiv$ quark. Therefore, as shown in Fig. 1, the two-step cascade DM annihilation process via the on-shell pseudoscalar boson into the SM particles are dominated by τ 's in the final states for a large $\tan \beta$. Note that the DM annihilation into tau's cannot be through the heavier on-shell neutral Higgs, which is kinematically forbidden, because, as shown in this work, its mass $m_H \sim 300$ GeV is much larger than the DM mass. Note also that, in contrast with the type-X case, for the type-II Yukawa interactions, because both the down-type quark and lepton couplings of the heavier neutral Higgs boson are enhanced by $\tan \beta$, that model will be severely constrained by the extra Higgs search at the LHC and by the flavor physics [51].

In the present work, we study that the vector DM (X) first annihilates into the unstable hidden Higgs bosons (S), as shown in Fig. 2, and then the S dominantly decays into the pseudoscalar pair. In the following section, we will give the triple and quartic Higgs couplings, which are relevant to the $XX \rightarrow SS$ and $S \rightarrow AA$ processes. Moreover, these couplings are also relevant to the Boltzmann equations, which will be discussed in Sec. VB.

C. The triple and quartic Higgs couplings

We consider that the GC gamma-ray excess originates from the two-step cascade DM annihilation, so that the mixing angles, δ and θ , are small, and only terms linear in $\sin \delta$ and $\sin \theta$ are kept

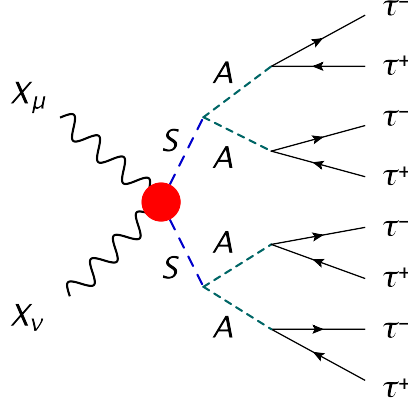


FIG. 1. The main DM annihilation process of two-step cascades, $X_\mu X_\nu \rightarrow SS \rightarrow 4A$'s $\rightarrow 8\tau$'s, relevant to the GC gamma-ray excess. The red shaded region contains interactions shown in Fig. 2.

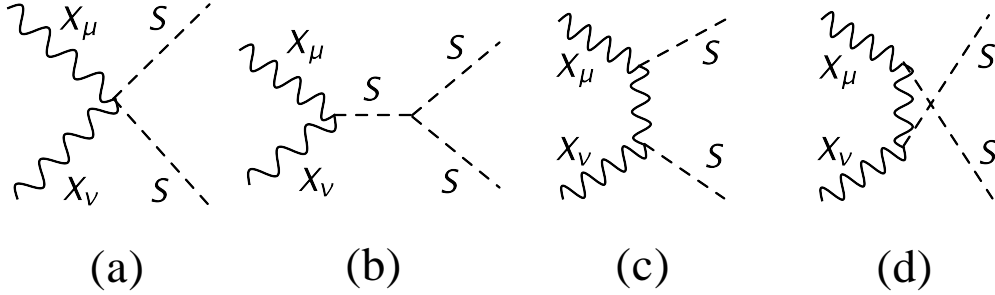


FIG. 2. Feynman diagrams that dominantly contribute to the DM annihilation cross section relevant to relic abundance and GC gamma-ray excess, where (a), (b), (c), and (d) are for the 4-vertex, s -, t -, u -channels, respectively.

in the effective couplings. However, because $\tan\beta$ needs to be larger (~ 35) in the present case, we also keep the terms, which are quadratic in these two angles and involve $\tan\beta$. The constraints on δ and θ will be discussed in Sec. V.

The Lagrangian, containing triple and quartic Higgs couplings, are relevant to the present study. Using the result given in Appendix B, we can express these couplings in terms of the squares of physical Higgs masses and M^2 as

$$\begin{aligned} \mathcal{L}_{\text{triple}} \supset & \frac{1}{2}v\lambda_{hAA}hAA + \frac{1}{2}v\lambda_{HAA}HAA + \frac{1}{2}v\lambda_{SAA}SAA + \frac{1}{2}v\lambda_{hSS}hSS + \frac{1}{2}v\lambda_{HSS}HSS \\ & + \frac{1}{6}v\lambda_{SSS}SSS + \dots, \end{aligned} \quad (13)$$

$$\mathcal{L}_{\text{quartic}} \supset \frac{1}{4}\lambda_{SSAA}SSAA + \frac{1}{24}\lambda_{SSSS}SSSS \dots, \quad (14)$$

where, neglecting all terms suppressed by s_δ^2 , s_θ^2 , and $s_\delta s_\theta$ except that enhanced by t_β , the couplings

are given by

$$\lambda_{hAA} \simeq \frac{1}{v^2} \left[(2M^2 - 2m_A^2 - m_h^2) s_{\beta-\alpha} - (M^2 - m_h^2) \left(t_\beta - \frac{1}{t_\beta} \right) c_{\beta-\alpha} \right], \quad (15)$$

$$\lambda_{HAA} \simeq \frac{1}{v^2} \left[(2M^2 - 2m_A^2 - m_H^2) c_{\beta-\alpha} + (M^2 - m_H^2) \left(t_\beta - \frac{1}{t_\beta} \right) s_{\beta-\alpha} \right], \quad (16)$$

$$\lambda_{SAA} \simeq \frac{1}{v^2} \left[-M^2 \left(\frac{c_\alpha s_\theta - s_\alpha s_\delta}{c_\beta} + \frac{s_\alpha s_\theta + c_\alpha s_\delta}{s_\beta} \right) + m_S^2 \left(s_\beta^2 \frac{c_\alpha s_\theta - s_\alpha s_\delta}{c_\beta} + c_\beta^2 \frac{s_\alpha s_\theta + c_\alpha s_\delta}{s_\beta} \right) \right. \\ \left. + 2m_A^2 \left((c_\alpha s_\theta - s_\alpha s_\delta) c_\beta + (s_\alpha s_\theta + c_\alpha s_\delta) s_\beta \right) \right], \quad (17)$$

$$\lambda_{hSS} \simeq -\frac{2m_S^2 + m_h^2}{vv_S} \left[s_\delta - (c_\alpha s_\theta - s_\alpha s_\delta)^2 s_\alpha \frac{t_\beta v_s}{s_\beta v} \right] \\ - \frac{3M^2 t_\beta (c_\alpha s_\theta - s_\alpha s_\delta)}{v^2 s_\beta} \left[(s_\alpha s_\theta + c_\alpha s_\delta) c_\alpha - s_\delta s_\beta^2 \right], \quad (18)$$

$$\lambda_{HSS} \simeq -\frac{2m_S^2 + m_h^2}{vv_S} \left[s_\theta + (c_\alpha s_\theta - s_\alpha s_\delta)^2 c_\alpha \frac{t_\beta v_s}{s_\beta v} \right] \\ - \frac{3M^2 t_\beta (c_\alpha s_\theta - s_\alpha s_\delta)}{v^2 s_\beta} \left[(s_\alpha s_\theta + c_\alpha s_\delta) s_\alpha - s_\theta s_\beta^2 \right], \quad (19)$$

$$\lambda_{SSS} \simeq -\frac{3m_S^2}{vv_S}, \quad (20)$$

$$\lambda_{SSAA} \simeq \frac{1}{vv_S} \left[s_\beta t_\beta \left(m_H^2 c_\alpha s_\theta - m_h^2 s_\alpha s_\delta - m_S^2 (c_\alpha s_\theta - s_\alpha s_\delta) \right) \right. \\ \left. + \frac{c_\beta}{t_\beta} \left(m_H^2 s_\alpha s_\theta + m_h^2 c_\alpha s_\delta - m_S^2 (s_\alpha s_\theta + c_\alpha s_\delta) \right) \right], \quad (21)$$

$$\lambda_{SSSS} \simeq \frac{3m_S^2}{v_S^2}. \quad (22)$$

Here and in the following, we adopt the abbreviations: $s_\sigma \equiv \sin \sigma$, $c_\sigma \equiv \cos \sigma$, and $t_\sigma \equiv \tan \sigma$.

D. The decay widths for the S and A bosons

The partial decay widths for S and A are relevant to the studies of the relic density and indirect detection searches. The partial decay widths of the S boson are

$$\Gamma(S \rightarrow \bar{f}f) = N_c^f \frac{m_S}{8\pi} \left(\frac{m_f}{v} \right)^2 |g_{Sff}|^2 \left(1 - \frac{4m_f^2}{m_S^2} \right)^{3/2} \theta(m_S - 2m_f), \quad (23)$$

$$\Gamma(S \rightarrow gg) = \frac{\alpha_s^2}{2\pi^3 m_S} \left| \sum_{q=\text{quarks}} \frac{m_q^2}{v} g_{Sq} f_S \left(\frac{4m_q^2}{m_S^2} \right) \right|^2, \quad (24)$$

$$\Gamma(S \rightarrow AA) = \frac{\lambda_{SAA}^2 v^2}{32\pi m_S} \left(1 - \frac{4m_A^2}{m_S^2} \right)^{1/2} \theta(m_S - 2m_A), \quad (25)$$

where $N_c^f \equiv 3$ (1) for quarks (leptons), and $f_S(\tau) = [1 + (1 - \tau)f(\tau)]$ with

$$f(\tau) = \begin{cases} \arcsin^2 \sqrt{\tau^{-1}}, & \tau \geq 1 \\ -\frac{1}{4} \left[\log \frac{1+\sqrt{1-\tau}}{1-\sqrt{1-\tau}} - i\pi \right]^2, & \tau < 1 \end{cases}. \quad (26)$$

The partial decay widths of the CP-odd boson A are given by

$$\Gamma(A \rightarrow \bar{f}f) = N_c^f \frac{m_A}{8\pi} \left(\frac{m_f}{v} \right)^2 |g_{Aff}|^2 \left(1 - \frac{4m_f^2}{m_A^2} \right)^{1/2} \theta(m_A - 2m_f), \quad (27)$$

$$\Gamma(A \rightarrow gg) = \frac{\alpha_s^2}{2\pi^3 m_A} \left| \sum_{q=\text{quarks}} \frac{m_q^2}{v} g_{Aqq} f \left(\frac{4m_q^2}{m_A^2} \right) \right|^2, \quad (28)$$

with the couplings $g_{A\tau\tau} = g_{A\mu\mu} = \tan\beta$, $|g_{Aqq}| = 1/\tan\beta$ in the consideration of the type-X Yukawa interactions. In the present case, because we take into account the large $\tan\beta$ (~ 35) and $m_A = 15 \sim 20$ GeV (see later discussions), we therefore have $\text{Br}(A \rightarrow \tau\tau) \simeq 1$, $\text{Br}(A \rightarrow \mu\mu) \simeq \text{Br}(A \rightarrow \tau\tau) \times (m_\mu/m_\tau)^2 \simeq 0.0035$, and neglect $A \rightarrow \bar{q}q$ and $A \rightarrow gg$ due to the $1/\tan^2\beta$ suppression in the decay rates.

III. USE OF THE PARAMETERS UNDER THE EXPERIMENTAL AND THEORETICAL CONSTRAINTS

For the CP-conserving LN2HDM, we adopt the observed Higgs resonance as one of the CP-even scalars: h with mass $m_h = 125.09$ GeV [52], $v^2 \equiv (\sqrt{2}G_F)^{-1} \simeq (246 \text{ GeV})^2$. Compared with the SM, the interactions contain 11 more independent parameters. We take the following remaining parameters as inputs:

$$\begin{aligned} g_X, \quad \tan\beta, \quad \beta - \alpha, \quad \theta, \quad \delta, \\ m_X, \quad m_S, \quad m_H, \quad m_A, \quad m_{H^\pm}, \quad M^2 \equiv m_{12}^2/(\sin\beta \cos\beta). \end{aligned} \quad (29)$$

In this parametrization, the tree-level couplings of the Higgs bosons to SM particles are functions of $\tan\beta$, $\beta - \alpha$, θ , and δ . In the following, we will experimentally and theoretically constrain the parameters relevant to the two-Higgs doublets and Yukawa sectors.

A. Experimental considerations

In the present paper, we consider that the GC gamma excess is mostly due to the two-step cascade annihilation of the dark matter into the final state τ 's, for which the main process is

schematically shown in Fig. 1, where the shaded region denotes the interactions, depicted in Fig. 2, and is relevant to the DM annihilation cross section. As shown in the following GC gamma-ray excess study that $m_A \sim 10 - 20 \text{ GeV} < m_h/2$, we therefore need to consider the constraint on $\text{Br}(h \rightarrow AA)$, which is proportional to the square of λ_{hAA} . The magnitude of λ_{hAA} can be constrained from the measurement of $\text{Br}(h \rightarrow AA \rightarrow 4\tau) \simeq \text{Br}(h \rightarrow AA)$, of which the current upper bound [53, 54] is about 0.2-0.4 for $8 \leq m_A \leq 30 \text{ GeV}$, resulting in $|\lambda_{hAA}| < 1.95 \times 10^{-2}$. Following Ref. [44], we will take $\lambda_{hAA} = 0$, i.e.,

$$(2M^2 - 2m_A^2 - m_h^2)s_{\beta-\alpha} = (M^2 - m_h^2) \left(t_\beta - \frac{1}{t_\beta} \right) c_{\beta-\alpha}, \quad (30)$$

from which, under the conditions of $t_\beta \gg 1$, $m_A^2/M^2 \ll 1$, $m_h^2/M^2 \ll 1$ and $s_{\beta-\alpha} \rightarrow 1$, one can obtain the following approximations,

$$\sin(\beta - \alpha) \simeq 1 - \frac{2}{\tan^2 \beta} \left(1 + \frac{m_h^2}{M^2} - \frac{2m_A^2}{M^2} \right), \quad (31)$$

$$\cos(\beta - \alpha) \simeq \frac{2}{\tan \beta} \left(1 + \frac{m_h^2}{2M^2} - \frac{m_A^2}{M^2} \right). \quad (32)$$

Using the results in Eqs. (31) and (32), the normalized Yukawa coupling of the SM Higgs to the lepton pair can be expressed as

$$\frac{g_{h\ell\ell}}{g_{h\ell\ell}^{\text{SM}}} = -\frac{s_\alpha}{c_\beta} = s_{\beta-\alpha} - t_\beta c_{\beta-\alpha} \simeq -1 - \frac{m_h^2}{M^2} + 2\frac{m_A^2}{M^2} - \frac{2}{t_\beta^2} \left(1 + \frac{m_h^2}{M^2} - \frac{2m_A^2}{M^2} \right). \quad (33)$$

In this case, the alignment limit, $s_{\beta-\alpha} \rightarrow 1$, reproduces the wrong-sign SM coupling $g_{h\ell\ell} \rightarrow -1$. Taking the combination of the ATLAS and CMS $h \rightarrow \tau\tau$ measurements, the signal strength reads $\mu_{\tau\tau} \equiv (\sigma_h \cdot \text{BR})_{\tau\tau}^{\text{obs}} / (\sigma \cdot \text{BR})_{\tau\tau}^{\text{SM}} = 1.11_{-0.22}^{+0.24}$ [55], which is defined as the observed product of the SM-like Higgs production cross section and the decay branching ratio $h \rightarrow \tau\tau$, normalized to the corresponding SM value. The corresponding requirement for $m_A \leq 20 \text{ GeV}$ is $|g_{h\tau\tau}| < 1.26$ at 2σ confidence level (C.L.), such that we have $M \gtrsim 245 \text{ GeV}$.

The masses of Higgs bosons can be constrained by the electroweak precision measurements. Such new physics effects, which contribute the gauge vacuum polarization at the one-loop level, can be described by three oblique parameters, S, U and T . We adopt the definition of these parameters, originally introduced by Peskin and Takeuchi [56, 57]. Taking the limit $s_{\beta-\alpha} \rightarrow 1$, $|m_{H^\pm} - m_H| \ll m_H$ and $m_A \ll m_H$, and keeping terms linear in $\sin \theta$ and $\sin \delta$, we obtain three oblique parameters from that given in Ref. [58], where a general multi-Higgs-doublet model was studied. The results are collected in Appendix C. In the limit that we take, the formulas are consistent with those in the two-Higgs doublet model, i.e. the correction due to the hidden Higgs

boson S is negligible, and the results approximately read

$$\begin{aligned}
S &\approx -\frac{1}{24\pi} \left(\frac{5}{3} + \frac{4(m_{H^\pm} - m_H)}{m_H} \right) \simeq -0.022 - 0.002 \times \frac{300 \text{ GeV}}{m_H} \frac{m_{H^\pm} - m_H}{10 \text{ GeV}}, \\
T &\approx \frac{1}{32\pi^2 \alpha_{\text{em}} v^2} m_H (m_{H^\pm} - m_H) \simeq 0.04 \times \frac{m_H}{300 \text{ GeV}} \frac{m_{H^\pm} - m_H}{10 \text{ GeV}}, \\
U &\approx \frac{1}{12\pi} \left(\frac{m_{H^\pm} - m_H}{m_H} \right) \simeq 0.001 \times \frac{300 \text{ GeV}}{m_H} \frac{m_{H^\pm} - m_H}{10 \text{ GeV}},
\end{aligned} \tag{34}$$

where the T parameter is especially sensitive to the mass splitting, $m_{H^\pm} - m_H$. For the values $m_H \approx 300 \text{ GeV}$ and $|m_{H^\pm} - m_H| \sim \mathcal{O}(10) \text{ GeV}$, the theoretical prediction is consistent with that from the data fit which gives [73]

$$S = 0.05 \pm 0.10, \quad T = 0.08 \pm 0.12, \quad U = 0.02 \pm 0.10. \tag{35}$$

B. Theoretical considerations

For this model, we need to have $m_H \sim m_{H^\pm} \sim M \gg m_A$. To satisfy the perturbative bound, we impose the absolute values of all the quartic couplings to be less than 4π . We can easily make the estimate on the mass bound for the heavy Higgs as follows. From Eq. (B5), we have $M^2 = \lambda_5 v^2 + m_A^2 < 4\pi v^2 + m_A^2$, so that $M^2 \lesssim (873 \text{ GeV})^2$ for $m_A \lesssim 40 \text{ GeV}$. From Eq. (B4), we get $m_{H^\pm}^2 = (M^2 - m_A^2 - \lambda_4 v^2)/2 \lesssim (873^2 + 4\pi \times 246^2)/2 \text{ GeV}^2$, i.e., $m_{H^\pm} \lesssim 873 \text{ GeV}$. For small mixing angles, θ and δ , which are relevant to the present work, the tree-level perturbative unitarity, as the case of the type-X 2HDM, gives $m_{H^\pm} \lesssim 700 \text{ GeV}$ [44]. On the other hand, the vacuum stability and perturbativity could be broken when we consider this model at higher scale, for which, again, in the limit of small θ and δ , the related bound is the same as the type-X 2HDM, and given by $m_{H^\pm} \lesssim (400) 310 \text{ GeV}$ for the cutoff scale $\Lambda \simeq (10) 100 \text{ TeV}$ [22, 44].

Neglecting the terms with power higher than that linear in s_θ and s_δ , and taking the limit $s_{\beta-\alpha} \rightarrow 1$ and $t_\beta \gg 1$, we have, from Eq. (B1), that

$$\begin{aligned}
m_H^2 - M^2 &\cong \frac{\lambda_1 v^2}{t_\beta^2} + (m_H^2 - m_h^2) c_{\beta-\alpha}^2 - 2(m_H^2 - m_h^2) \frac{s_{\beta-\alpha} c_{\beta-\alpha}}{t_\beta} - \frac{1}{t_\beta^2} (m_H^2 c_{\beta-\alpha}^2 + m_h^2 s_{\beta-\alpha}^2) \\
&\simeq \frac{\lambda_1 v^2}{t_\beta^2} - \frac{2m_H^2}{t_\beta^2} \left(\frac{m_h^2}{M^2} - \frac{2m_A^2}{M^2} \right) + \frac{m_h^2}{t_\beta^2} \left(1 + \frac{2m_h^2}{M^2} - \frac{4m_A^2}{M^2} \right),
\end{aligned} \tag{36}$$

where the second line is obtained by using the relations given in Eqs. (31) and (32). Considering the perturbativity and vacuum stability requirements: $0 < \lambda_1 < 4\pi$, we can get $m_H - M \simeq \lambda_1 v^2 / (2m_H t_\beta^2) \lesssim 1 \times \frac{300 \text{ GeV}}{m_H} \text{ GeV}$ for a large $\tan \beta \gtrsim 35$ and $m_H \gtrsim 250 \text{ GeV}$.

IV. COSMOLOGICAL AND ASTROPHYSICAL CONSTRAINTS

A. The gamma-ray spectrum originating from the two-step cascade dark matter annihilations: determining m_X, m_S , and m_A

The *differential gamma-ray flux*, arising from the two-step cascade annihilations of the vector DM, can be expressed by

$$\frac{d\Phi_\gamma}{dE} = \frac{1}{8\pi m_X^2} \sum_f \langle \sigma v \rangle_f \left(\frac{dN_\gamma^f}{dE} \right)_X \underbrace{\frac{1}{\Delta\Omega} \int_{\Delta\Omega} \int_{\text{l.o.s.}} ds \rho^2(r(s, \psi)) d\Omega}_{\text{J-factor}}, \quad (37)$$

where the J-factor is the integral of the DM density squared along the line of sight (l.o.s.) and over the solid angle $\Delta\Omega$ that covers the region of interest (ROI), and $\langle \sigma v \rangle_f$ and $(dN_\gamma^f/dE)_X$ are the low-velocity averaged annihilation cross section and the gamma-ray spectrum produced per annihilation with final state f , respectively. For illustration, the dominant process is depicted in Fig. 1, where the final states are τ 's, which mainly arise from the process, $\langle \sigma v \rangle_\tau \simeq \langle \sigma v \rangle_{XX \rightarrow SS} \times \text{Br}(S \rightarrow AA) \times \text{Br}(A \rightarrow \tau\tau)$, with $\text{Br}(S \rightarrow AA) \simeq 1$ and $\text{Br}(A \rightarrow \tau\tau) \simeq 1$. Following the method given in Ref. [41], we can perform two-step Lorentz boosts to transform the gamma-ray spectrum given in the A boson rest frame, $(dN_\gamma^\tau/dE)_A$, to the XX center of mass (CM) frame; we first boost the spectrum to the S rest frame and then to the CM frame of the XX pair. For $(dN_\gamma^\tau/dE)_A$, we will use the PPPC4DMID result [59, 60], which was generated by using PYTHIA 8.1 [61]. Thus, $(dN_\gamma^\tau/dx_2)_X = m_X (dN_\gamma^\tau/dE)_X$ can be written as

$$\left(\frac{dN_\gamma^\tau}{dx_2} \right)_X = 4 \int_{t_{2,\min}}^{t_{2,\max}} \frac{dx_1}{x_1 \sqrt{1 - \epsilon_2^2}} \int_{t_{1,\min}}^{t_{1,\max}} \frac{dx_0}{x_0 \sqrt{1 - \epsilon_1^2}} \left(\frac{dN_\gamma^\tau}{dx_0} \right)_A, \quad (38)$$

where

$$\epsilon_2 = \frac{m_S}{m_X}, \quad \epsilon_1 = \frac{2m_A}{m_S}, \quad (39)$$

$$0 \leq x_2 \leq \frac{1}{4} \left(1 + \sqrt{1 - \epsilon_1^2} \right) \left(1 + \sqrt{1 - \epsilon_2^2} \right), \quad x_2 = \frac{E}{m_X}, \quad x_1 = \frac{2E_1}{m_S}, \quad x_0 = \frac{2E_0}{m_A}, \quad (40)$$

$$t_{1,\max} = \min \left[1, \frac{2x_1}{\epsilon_1^2} \left(1 + \sqrt{1 - \epsilon_1^2} \right) \right], \quad t_{1,\min} = \frac{2x_1}{\epsilon_1^2} \left(1 - \sqrt{1 - \epsilon_1^2} \right), \quad (41)$$

$$t_{2,\max} = \min \left[\frac{1}{2} \left(1 + \sqrt{1 - \epsilon_1^2} \right), \frac{2x_2}{\epsilon_2^2} \left(1 + \sqrt{1 - \epsilon_2^2} \right) \right], \quad t_{2,\min} = \frac{2x_2}{\epsilon_2^2} \left(1 - \sqrt{1 - \epsilon_2^2} \right), \quad (42)$$

with E , E_1 , and E_0 being the photon energies in the XX CM frame, S rest frame, and A rest frame, respectively.

B. The Galactic Center gamma-ray excess

We use the GC gamma-ray excess spectrum obtained by CCW [8], who have studied Fermi-LAT data covering the energy range 300 MeV–500 GeV in the inner Galaxy, where the ROI extended to a $40^\circ \times 40^\circ$ square region around the GC with the inner latitude less than 2° masked out. The systematic uncertainties of the background have been taken into account by CCW through a large number of Galactic diffuse emission models.

To see whether the present vector DM model can meet the observation, we perform a goodness-of-fit test, by calculating the χ^2 test statistic,

$$\chi^2 = \sum_{ij \in \text{bins}} \left[\frac{d\Phi_\gamma}{dE_i}(m_X, \langle\sigma v\rangle) - \left(\frac{d\Phi_\gamma}{dE_i} \right)_{\text{obs}} \right] \cdot \Sigma_{ij}^{-1} \cdot \left[\frac{d\Phi_\gamma}{dE_j}(m_X, \langle\sigma v\rangle) - \left(\frac{d\Phi_\gamma}{dE_j} \right)_{\text{obs}} \right], \quad (43)$$

where 24 energy bins are adopted in the range 300 MeV–500 GeV, $d\Phi_\gamma/dE_i$ and $(d\Phi_\gamma/dE_i)_{\text{obs}}$ are the model-predicted and observed flux in the i th bin, respectively. Here the covariance Σ_{ij} contains the uncorrelated statistical error, and correlated uncertainties, of which the latter is composed of the empirical model systematics and residual systematics. Although CCW performed the analysis using the older Fermi dataset, however, it was shown in Ref. [62] that the results have very little changes between Fermi Pass 7 and newer Pass 8 data. This appreciable difference at low energies might be due to the modeling for the point sources in various datasets [11, 62]. On the other hand, it is interesting to note that the central values of the low energy spectrum given by [11] seem to be smaller than that obtained by CCW. If so, the best-fit DM mass will become larger compared with the present result.

Two physical parameters, $\langle\sigma v\rangle$ and m_X , can thus be obtained from the fit. The value of $\langle\sigma v\rangle$ is sensitive to the form of the Galactic DM density distribution, for which we use a generalized Navarro-Frenk-White (gNFW) halo profile [63, 64],

$$\rho(r) = \rho_\odot \left(\frac{r}{r_\odot} \right)^{-\gamma} \left(\frac{1 + r/r_s}{1 + r_\odot/r_s} \right)^{\gamma-3}, \quad (44)$$

where the scale radius $r_s = 20$ kpc, r is the distance to the GC, $-\gamma$ is the inner log slope of the halo density near the GC, and ρ_\odot is the local DM density at $r_\odot = 8.5$ kpc, which is the radial distance of the Sun from the GC. We will take $\gamma = 1.2$ and $\rho_\odot = 0.357$ GeV as the canonical values. However, the uncertainties about the local dark matter density and the halo distribution near the GC remains large. The resulting annihilation cross section in the fit due to the variation of $\gamma \in [1.1, 1.3]$ and $\rho_\odot \in [0.2, 0.6]$ GeV will be discussed later.

C. The constraint from dwarf spheroidal observations

In the present analysis, we will use the combined gamma-ray data of 28 confirmed and 17 candidate dwarf spheroidal galaxies (dSphs), recently reported by the Fermi-LAT and DES Collaborations [65, 66]. Compared with the earlier Fermi-Lat analysis [67], where some point-like sources were modeled as extended ones, a consistent analysis across 45 targets were presented in Ref. [65], and a limit weaker by a factor of ~ 1.5 were obtained in the low DM mass region ($\lesssim 70$ GeV). Because there is no gamma-ray signal detected so far from this kind of objects, a bound on the DM annihilation can thus be set.

We perform a combined likelihood analysis of 45 confirmed and candidate dSphs with 6 years of Fermi-LAT Pass 8 data in the energy range from 500 MeV to 500 GeV. The log-likelihood test statistic (TS) is given by

$$\text{TS} = -2 \sum_{k=1}^{N_{\text{dSph}}} \ln \left[\frac{\mathcal{L}_k(\langle\sigma v\rangle, \hat{J}_k; m_X | \text{data})}{\mathcal{L}_k(\overline{\langle\sigma v\rangle}, \bar{J}_k; m_X | \text{data})} \right], \quad (45)$$

with $N_{\text{dSph}} = 45$ and the profile likelihood of an individual target k ,

$$\mathcal{L}_k(\langle\sigma v\rangle, J_k; m_X | \text{data}) = \left(\sum_{i=1}^{N_{\text{bin}}} \mathcal{L}_{ki}(\langle\sigma v\rangle, J_k; m_X | \text{data}) \right) \cdot \mathcal{L}_{J_k}, \quad (46)$$

where $N_{\text{bin}} = 24$ are the numbers of bins, \mathcal{L}_{ki} is the i -th binned likelihood of the target k [66], and the J-factor likelihood for a target k is modeled by a normal distribution [68],

$$\mathcal{L}_{J_k} = \frac{1}{\ln(10) J_{o,k} \sqrt{2\pi} \sigma_k} e^{-(\log_{10} J_k - \log_{10} J_{o,k})^2 / (2\sigma_k^2)}. \quad (47)$$

Here, J_k is the expected J-factor of a target k , while the nominal value $J_{o,k}$ together with its error σ_k is the spectroscopically determined value when possible, or the predicted one from the distance scaling relationship with an uncertainty of 0.6 dex, otherwise [65]. For a given m_X , $\overline{\langle\sigma v\rangle}$ and \bar{J}_k are the maximum likelihood estimators (MLEs), which maximize $\sum_{k=1}^{N_{\text{dSph}}} \ln \mathcal{L}_k$. When $\langle\sigma v\rangle$ is fixed to a given value, \hat{J}_k are the conditional MLEs of the nuisance parameters. We can obtain the 95% confidence level (C.L.) limit on low-velocity annihilation cross section $\langle\sigma v\rangle$ from the null measurement by increasing its value from $\overline{\langle\sigma v\rangle}$ until $\text{TS} = 2.71$.

D. Results

In Fig. 1, we have depicted the two-step cascade DM annihilation process into the final state τ 's, which is the dominant mechanism to explain the GC gamma-ray excess in the present study.

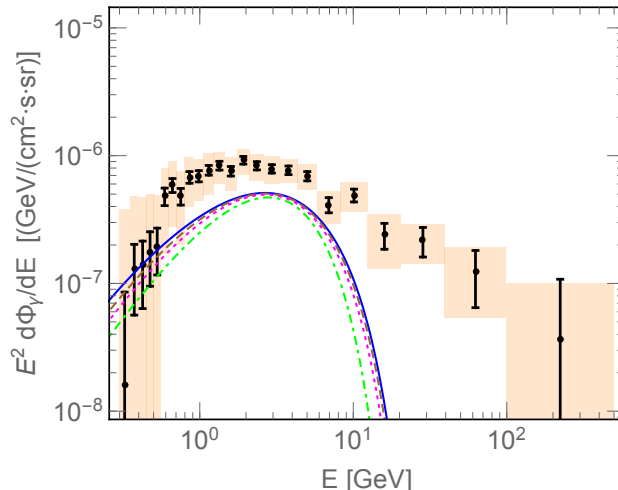


FIG. 3. Comparison of the spectrum of the Galactic Center gamma-ray excess [8] vs. the best-fit results for DM annihilating through a two-step cascade to the final state τ 's, where, for the former, the statistical and systematic errors are shown by error bars and orange rectangles, respectively, while for the latter, the solid (blue), dashed (brown), dotted (magenta), and dot-dashed (green) curves are for the cases of $(m_S, m_A) = (0.5m_X, 0.2m_X)$, $(0.7m_X, 0.3m_X)$, $(0.9m_X, 0.36m_X)$, and $(0.95m_X, 0.45m_X)$, respectively, with the corresponding p -values 0.22, 0.22, 0.23, 0.12. The corresponding good fit results, featuring by the p -values, are shown in the plane of m_X and low-velocity annihilation cross section in Fig. 4.

The DM annihilation diagrams, relevant to the indirect search and also to the relic abundance, are shown in Fig. 2; the resulting cross sections and related discussions are collected in Appendix D.

The DM two-step cascade annihilation process, increasing the final gamma-ray multiplicity and therefore resulting in a broader gamma-ray spectrum, provides a better fit to the GC data compared with that obtained from the DM annihilation directly into the tau pair. For illustration, in Fig. 3, we show the GC gamma-ray energy spectrum [8] compared our the best-fit model prediction. The corresponding GC fitted regions, featuring by the p -values, are shown in Fig. 4 on the plane of m_X and low-velocity annihilation cross section for four cases of $(m_S, m_A) = (0.5m_X, 0.2m_X)$, $(0.7m_X, 0.3m_X)$, $(0.9m_X, 0.36m_X)$, and $(0.95m_X, 0.45m_X)$, where $\rho_\odot = 0.357 \text{ GeV}/\text{cm}^3$ and $\gamma = 1.2$ have been adopted, so that the best GC fit is consistent with the WIMP relic abundance. The gauge coupling constant g_X in this model can thus be determined, and given as a function of m_X in Fig. 5. Note that, because the decay width of S is much less than m_S and, on the other hand, the annihilation $XX \rightarrow SS$ via an s -channel h or H exchange is highly suppressed, these two effects can be negligible. The detailed discussion will be given in Sec. V A. We find that this model can provide a good fit to the GC gamma-ray excess spectrum for the regions with

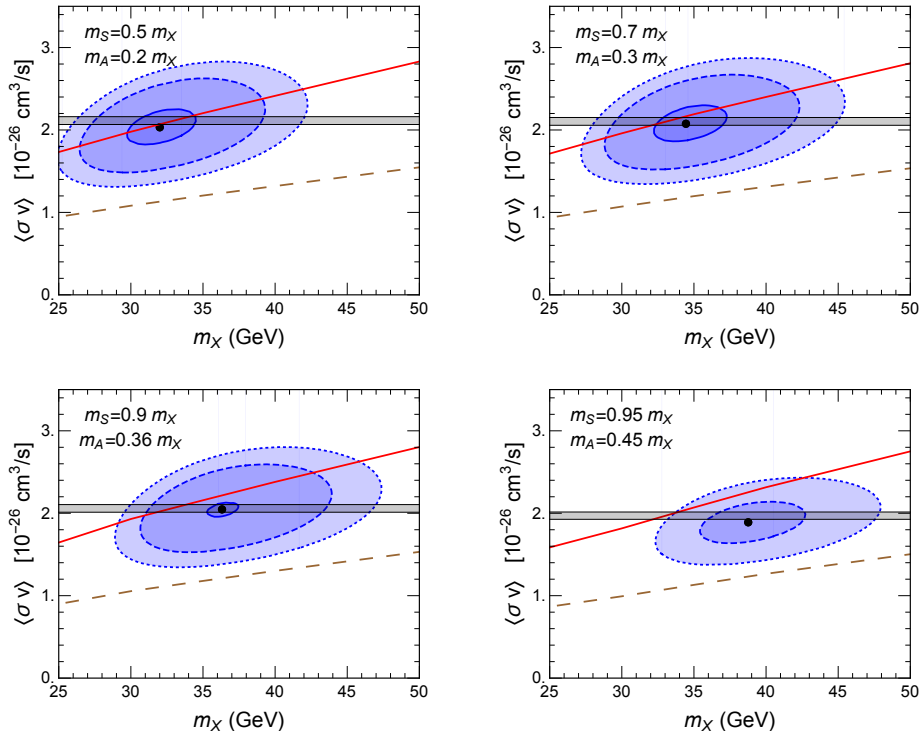


FIG. 4. Allowed parameter regions in the dark matter mass m_X and low-velocity annihilation cross section $\langle\sigma v\rangle$ plane. The GC fitted regions, shown in the blue color with solid, dashed and dotted boundaries, satisfy p -value $\geq 0.2, 0.1, 0.05$, respectively. The black dot marks the GC best-fit point. In conventional WIMP scenario, the thermal relic density can be accounted for by the narrowed grey region. All GC results refer to $\rho_\odot = 0.357 \text{ GeV/cm}^3$ and $\gamma = 1.2$. The 95% C.L. upper bound and projected limit from Fermi-LAT observations of dSphs are denoted as the solid red and long-dashed brown lines, respectively.

$m_X \sim 28 - 37$ (25 - 50) GeV, $m_A \sim 4 - 13$ (3.6 - 25) GeV and $m_X \gtrsim m_S \gtrsim 2m_A$, where p -value could be $\gtrsim 0.2$ (0.05).

Compared with the DM annihilation directly into the tau pair, the two-step cascades increase the final gamma-ray multiplicity by a factor of ~ 4 , such that if the dark matter mass is still the same, the resulting energy of the GeV photon peak will be reduced by a factor ~ 4 . Therefore, to fit the observed GeV gamma-ray excess, we need to increase m_X , i.e. the initial energy, by a factor ~ 4 in magnitude. On other hand, having the resulting changes for the final photon multiplicity and m_X , we thus know from Eq. (37) that the annihilation cross section also needs to be enlarged by a factor of ~ 4 to fit the gamma-ray spectrum.

Figs. 4 and 5 show the current 95% C.L. upper bound and projected limit from the gamma-ray observations of dSphs. The projected limit approximately rescales with the square root of the data

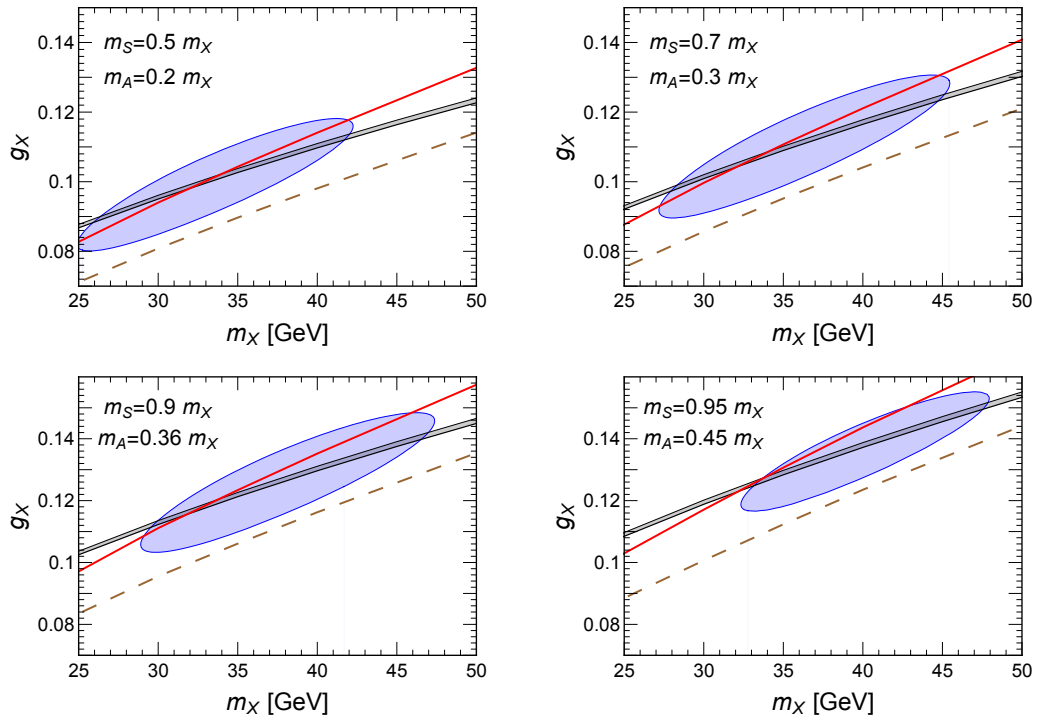


FIG. 5. Same as Fig. 4, but in the (m_X, g_X) plane, where the blue shaded region delineated with the blue line provides a good fit to the GC gamma-ray data with p -value ≥ 0.05 .

size and the square root of the number of targets [69]. Following the estimate given in Ref. [70], we conservatively assume that the 15-yr gamma-ray emission data can be successfully collected from the observation of 60 dSphs. Thus, the projected sensitivity on the $\langle\sigma v\rangle$ will be further improved by a factor of ~ 1.83 , and, as shown in Figs. 4 and 5, the present model is very likely to be probed in the near future.

In Figs. 4 and 5, we also show the region which is allowed by the correct DM relic abundance in the conventionally thermal WIMP scenario, for which we have rescaled the thermally averaged annihilation cross section at freeze-out temperature to its corresponding value defined at the low-velocity limit, where the effective number of degrees of freedom (DoF) $g_* \simeq 85.5$ corresponding to $T \simeq 1.9$ GeV (and $x \equiv m_X/T \simeq 22$) is adopted [71, 72]. Note that for a too small coupling constant λ_{SAA} , the S particle cannot maintain its chemical equilibrium with the thermal bath, such that the dark sector particles to be out of equilibrium with the bath when $T \lesssim m_{X(S)}$. For this case, we will show in Sec. VB that the allowed DM annihilation cross section to have the relic abundance could be (much) larger than that in the conventional WIMP scenario.

Three remarks for the gamma-ray fit are in order here. First, for the two-step cascade process,

the kinematical condition, $m_X \geq m_S \geq 2m_A \geq 4m_\tau$, needs to be satisfied. Second, considering variation of the local dark matter density from 0.357 to 0.2 (or 0.6) GeV/cm^3 and the halo slope γ from 1.2 to 1.1 (or 1.3), the low-velocity annihilation cross section and g_X in the GC gamma-ray fit would be further raised (or lowered) by factors of 4.10 and $\sim 4.10^{1/4}$ (or 0.27 and $\sim 0.27^{1/4}$), respectively. Third, the uncertainties of the observed J values of dSphs are subject to determination of DM mass profile which is assumed to be spherically symmetric and to have negligible binary motions [68].

V. DETERMINATION OF MIXING ANGLES, θ AND δ

A. Constraints from invisible Higgs decays and two-step cascade annihilation

Taking into account the GC gamma-ray excess which results from the two-step cascade annihilations of the vector dark matter into the final state τ 's in this model, we have found that the mass of dark matter lies within $25 \sim 50$ GeV, along with $m_S \lesssim m_X$ and $m_A \lesssim m_S/2$, as shown in Figs. 4 and 5. Therefore, because $m_h > 2m_S$, the decay $h \rightarrow SS$ is allowed and is followed by $S \rightarrow AA$ and subsequently $A \rightarrow \tau^+\tau^-$. This is relevant for search for the exotic Higgs decay with 8 τ 's in the final state. The exotic Higgs decays with 4 τ 's or other modes in the final state was discussed in Ref. [54]. Here and in the following sections, we will take parameters,

$$\begin{aligned} m_X &= 40 \text{ GeV}, m_S = 35 \text{ GeV}, m_A = 15 \text{ GeV}, \\ m_H &= m_{H^\pm} = M = 300 \text{ GeV}, g_X = 0.123, \tan \beta = 35, \beta - \alpha = 0.062909, \end{aligned} \quad (48)$$

as a benchmark in the discussions, and we have $\lambda_{hAA} \simeq 0$, $\text{Br}(h \rightarrow AA) \simeq 0$ due to the adopted values of $\tan \beta$ and $\beta - \alpha$. In Fig. 6, we show the contour plot for $\text{Br}(h \rightarrow SS)$ on the (θ, δ) plane, in comparison with a 95% C.L. limit: $\text{Br}(h \rightarrow \text{beyond SM}) < 34\%$, which was fitted with the Higgs produced via SM couplings [73].

A more stringent constraint can be obtained by requiring that the two-step cascade annihilation to the final state τ 's is dominant over the one-step cascade process described by the s -channel $XX \rightarrow AA$ followed by $A \rightarrow \tau^+\tau^-$. For this requirement, we will therefore restrict $\langle \sigma v \rangle_{XX \rightarrow AA} / \langle \sigma v \rangle_{XX \rightarrow SS}$ be to less than 0.05. Because the s -channel contributes about 15% to the total $XX \rightarrow SS$ cross section, we thus need to have $|\lambda_{SAA} / \lambda_{SSS}| \lesssim 0.48$ and $|\lambda_{SAA}| \lesssim 0.022$ (see also Fig. 6), where $\lambda_{SSS} = -3g_X m_S^2 / (m_X v) \simeq -0.046$. Imposing the constraints required by

$\text{Br}(h \rightarrow \text{beyond SM}) < 34\%$ and $|\lambda_{SAA}| \lesssim 0.022$, we then obtain

$$|\theta| \lesssim 0.001, \quad |\delta| \lesssim 0.088. \quad (49)$$

There may exist points with $\lambda_{SAA} \simeq 0$ on the (θ, δ) plane for $\delta \neq 0$. If we avoid this tiny region around that points, where the other decay modes are also highly suppressed due to the very small values of θ and δ , we always have $\text{Br}(S \rightarrow AA) \simeq 1$. In Fig. 6, the contour plot for the $S \rightarrow AA$ decay width is shown on the (θ, δ) plane. In this (two-step cascade annihilation dominant) case, we have $\Gamma_S/m_S \lesssim 6.7 \times 10^{-4}$ for $|\theta| \lesssim 0.001$, where Γ_S is the total width of the S boson; the value of the width can thus be negligible in the calculation. On the other hand, compared with $XX \rightarrow SS$ via an s -channel S exchange, as shown in Fig 2(b), if the mediator is replaced by h (or H), the resulting cross section is suppressed not only by the propagator of the heavier boson but also by the couplings squared: $(s_\delta \lambda_{hSS}/\lambda_{SSS})^2$ (or $(s_\theta \lambda_{HSS}/\lambda_{SSS})^2$), where s_δ (or s_θ) comes from the X - X - h (or X - X - H) vertex, and the coupling ratios $\lambda_{hSS}/\lambda_{SSS}$ and $\lambda_{HSS}/\lambda_{SSS}$ are shown in Fig. 6. Therefore, the annihilation $XX \rightarrow SS$ via a heavier mediator, h or H , is negligible in the calculation; the conclusion is also valid for the 0-step cascade annihilation via an s -channel h (or H) exchange since these cross sections are also suppressed by a factor of s_δ^2 (or s_θ^2) resulted from the X - X - h (or X - X - H) vertex.

In Fig. 6, we show the contour results of λ_{SAA} and $\lambda_{SAA}/\lambda_{SSS}$ on the (θ, δ) plane. As indicated in the relevant (θ, δ) region, the λ_{SAA} is much more sensitive to the variation of θ , compared with its dependence on δ . In the following analysis, the δ is simply set to be zero, and the dependence of the DM relic density on the effective coupling can be related to the variation of θ . If taking $\delta = 0$, the constraint from the two-step cascade annihilation gives $|\theta| \lesssim 0.00043$. Our conclusion can be easily extended to the case with $\delta \neq 0$.

B. Constraints from dark matter freeze-out and relic abundance

1. Coupled Boltzmann equations with interactions: $XX \leftrightarrow SS$, $SS \leftrightarrow AA$, and $S \leftrightarrow AA$

The interplay of the DM particles and SM particles mostly results from the interaction $XX \leftrightarrow SS$ followed by $S \leftrightarrow AA$ and $SS \leftrightarrow AA$ together with $A \leftrightarrow \tau^+\tau^-$ and $AA \leftrightarrow \tau^+\tau^-$. For $SS \rightarrow AA$ and $AA \rightarrow \tau^+\tau^-$, their annihilation cross sections are summarized in Appendix D 2, while for $S \rightarrow AA$ and $A \rightarrow \tau^+\tau^-$, their partial decay widths are given in Eqs. (23)-(28). Note that when the hidden sector particles become nonrelativistic at temperatures $T \lesssim m_{X,S}$, the cannibal annihilations could play important roles; such effects will be separately discussed in Sec. VB 2.

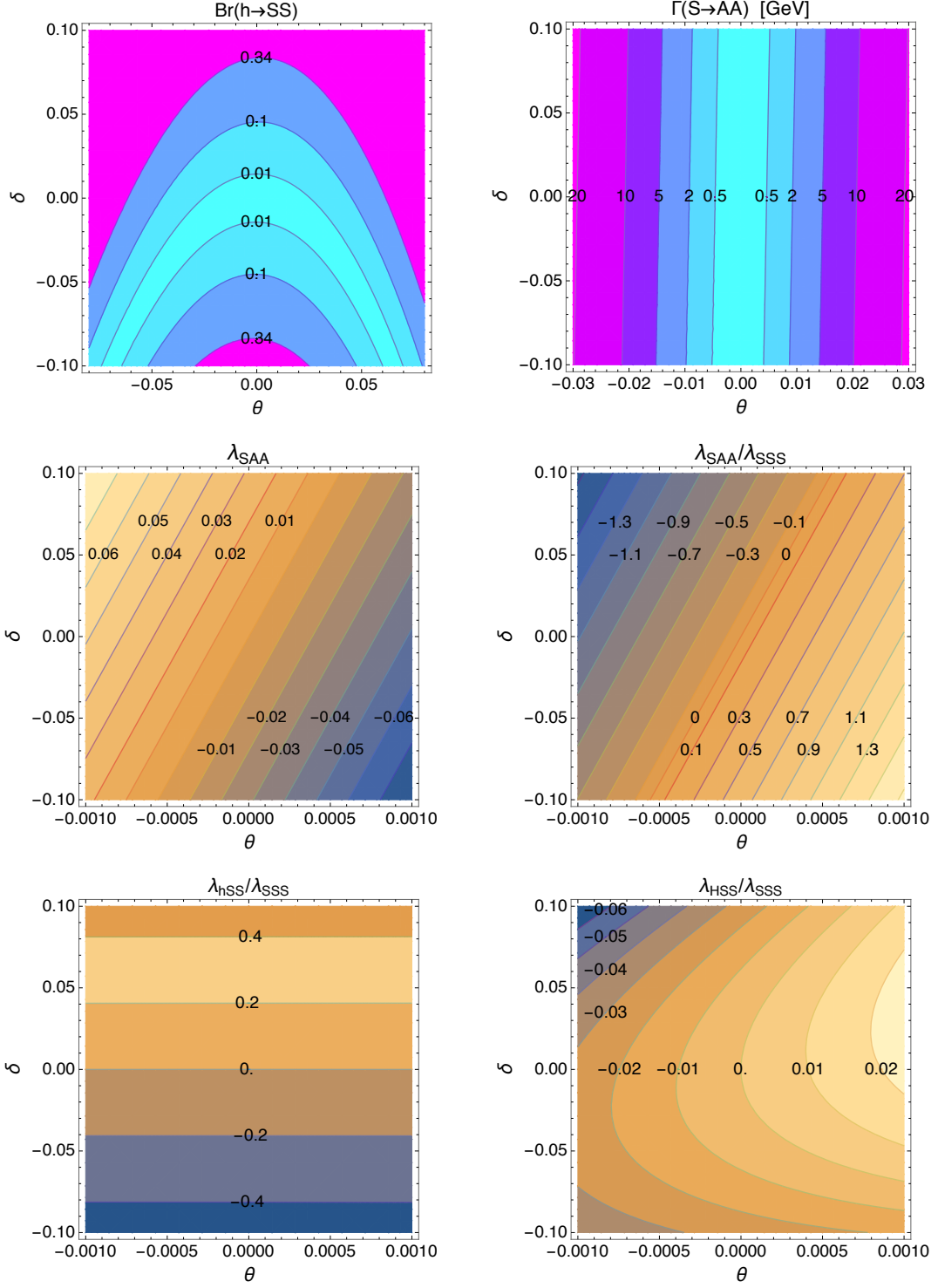


FIG. 6. The contour plots on the (θ, δ) plane for $\text{Br}(h \rightarrow SS)$, $\Gamma(S \rightarrow AA)$, λ_{SAA} , $\lambda_{SAA}/\lambda_{SSS}$, $\lambda_{hSS}/\lambda_{SSS}$, and $\lambda_{HSS}/\lambda_{SSS}$, where the parameters given in Eq. (48) are taken.

The evolutions of the number densities, n_X and n_S , for X and S , respectively, are described by

the coupled Boltzmann equations,

$$\frac{dn_X}{dt} + 3Hn_X = -\langle\sigma v\rangle_{XX\rightarrow SS}\left(n_X^2 - (n_X^{\text{eq}})^2\frac{n_S^2}{(n_S^{\text{eq}})^2}\right), \quad (50)$$

$$\begin{aligned} \frac{dn_S}{dt} + 3Hn_S = & -\langle\Gamma\rangle_{S\rightarrow AA}\left(n_S - n_S^{\text{eq}}\frac{n_A^2}{(n_A^{\text{eq}})^2}\right) - \langle\sigma v\rangle_{SS\rightarrow AA}\left(n_S^2 - (n_S^{\text{eq}})^2\frac{n_A^2}{(n_A^{\text{eq}})^2}\right) \\ & - \langle\sigma v\rangle_{SS\rightarrow XX}\left(n_S^2 - (n_S^{\text{eq}})^2\frac{n_X^2}{(n_X^{\text{eq}})^2}\right), \end{aligned} \quad (51)$$

where n_i^{eq} is the equilibrium number density for the particle “ i ”, and $\langle\sigma v\rangle$ and $\langle\Gamma\rangle$ are respectively the thermally averaged cross section and decay rate, corresponding to the specific process denoted in the subscript. For the present vector DM+type-X N2HDM, the interaction between the CP-odd Higgs boson A and lepton τ , via $A \leftrightarrow \tau^+\tau^-$ and $AA \leftrightarrow \tau^+\tau^-$, is strong enough to maintain the chemical and thermal equilibrium between A and the SM particles in the early Universe until the DM is completely freeze-out, i.e., $n_A = n_A^{\text{eq}}$; in other words, during the relevant epoch, like other SM particles, the A boson is in thermal equilibrium with the reservoir. On the other hand, the interaction strength between S and A depends on the effective coupling λ_{SAA} , which is a function of θ and δ (see also Fig. 6).

To solve Eqs. (50) and (51), we define the normalized yields,

$$y_X(x) = \sqrt{\frac{\pi}{45G}}m_X g_*^{1/2}\langle\sigma v\rangle_{XX\rightarrow SS}Y_X(x), \quad (52)$$

$$y_S(x) = \sqrt{\frac{\pi}{45G}}m_X g_*^{1/2}\langle\sigma v\rangle_{XX\rightarrow SS}Y_S(x), \quad (53)$$

where $Y_X \equiv n_X/s$ and $Y_S \equiv n_S/s$ are respectively the dark matter and mediator number densities normalized by the total entropy density, $g_*^{1/2} = h_{\text{eff}}[1 + (1/3)(d \ln h_{\text{eff}}/d \ln T)]/g_{\text{eff}}^{1/2}$ is the effectively total number of relativistic DoF, and $x \equiv m_X/T$ is the variable that will be used instead of time t . Here g_{eff} and h_{eff} are the effective DoF for the energy density and entropy density, respectively [71]. Using the new defined quantities, we can rewrite these two Boltzmann equations into the following forms

$$\frac{dy_X}{dx} = -\frac{1}{x^2}\left(y_X^2 - (y_X^{\text{eq}})^2\frac{y_S^2}{(y_S^{\text{eq}})^2}\right), \quad (54)$$

$$\begin{aligned} \frac{dy_S}{dx} = & -x\frac{\sqrt{90}}{\pi}M_{\text{pl}}\frac{g_*^{1/2}}{h_{\text{eff}}}\frac{\langle\Gamma\rangle_{S\rightarrow AA}}{m_X^2}(y_S - y_S^{\text{eq}}) - \frac{1}{x^2}\frac{\langle\sigma v\rangle_{SS\rightarrow AA}}{\langle\sigma v\rangle_{XX\rightarrow SS}}\left[y_S^2 - (y_S^{\text{eq}})^2\right] \\ & - \frac{1}{x^2}\frac{\langle\sigma v\rangle_{SS\rightarrow XX}}{\langle\sigma v\rangle_{XX\rightarrow SS}}\left(y_S^2 - (y_S^{\text{eq}})^2\frac{y_X^2}{(y_X^{\text{eq}})^2}\right), \end{aligned} \quad (55)$$

where $M_{\text{pl}} = (8\pi G)^{-1/2} = 2.44 \times 10^{18}$ GeV is the reduced Planck mass, and the values of y_i in equilibrium are given by

$$y_i^{\text{eq}}(x) = g_i\frac{\sqrt{90}}{2\pi^3}M_{\text{pl}}\frac{g_*^{1/2}}{h_{\text{eff}}}m_X\left(x\frac{m_i}{m_X}\right)^2\langle\sigma v\rangle_{XX\rightarrow SS}K_2\left(x\frac{m_i}{m_X}\right), \quad (56)$$

with the subscript index “ i ” $\equiv X$ or S , and $g_X = 3$ and $g_S = 1$ being the internal degrees of freedom of the X (dark matter) and S (mediator) particles, respectively. Using the relations, which are inferred from the Boltzmann equation [74],

$$(y_X^{\text{eq}})^2 \langle \sigma v \rangle_{XX \rightarrow SS} = (y_S^{\text{eq}})^2 \langle \sigma v \rangle_{SS \rightarrow XX}, \quad (57)$$

$$\langle \Gamma \rangle_{S \rightarrow AA} = \Gamma_{S \rightarrow AA} \frac{K_1(x \cdot m_S/m_X)}{K_2(x \cdot m_S/m_X)}, \quad (58)$$

where $\Gamma_{S \rightarrow AA}$ is the $S \rightarrow AA$ decays width given in the rest frame of S , and K_i is the modified Bessel function of second kind, we can further recast Eq. (55) into the form,

$$\begin{aligned} \frac{dy_S}{dx} = & -x \frac{\sqrt{90}}{\pi} M_{\text{pl}} \frac{g_*^{1/2}}{h_{\text{eff}}} \frac{\Gamma_{S \rightarrow AA}}{m_X^2} \frac{K_1(x \cdot m_S/m_X)}{K_2(x \cdot m_S/m_X)} (y_S - y_S^{\text{eq}}) - \frac{1}{x^2} \frac{\langle \sigma v \rangle_{SS \rightarrow AA}}{\langle \sigma v \rangle_{XX \rightarrow SS}} \left[y_S^2 - (y_S^{\text{eq}})^2 \right] \\ & - \frac{1}{x^2} \left[\frac{(y_X^{\text{eq}})^2}{(y_S^{\text{eq}})^2} y_S^2 - y_X^2 \right]. \end{aligned} \quad (59)$$

Because both the annihilation processes, $SS \rightarrow AA$ and $XX \rightarrow SS$, occur through the s-wave, for simplicity, in the following discussion we approximate $\langle \sigma v \rangle_{SS \rightarrow AA} \simeq \langle \sigma v \rangle_{SS \rightarrow AA}^{(0)}$ and $\langle \sigma v \rangle_{XX \rightarrow SS} \simeq \langle \sigma v \rangle_{XX \rightarrow SS}^{(0)}$ using their leading values in $v \rightarrow 0$ limit. Note that in the Boltzmann equation, the contribution due to the $SS \leftrightarrow AA$ interaction is usually much smaller than the process $S \leftrightarrow AA$; in other words, in Eq. (59), the second term of the right hand side (RHS) is negligible, especially when the co-decay occurs with $|\lambda_{SAA}| \lesssim 1.03 \times 10^{-8}$, corresponding to $|\theta| \lesssim 2 \times 10^{-10}$ if $\delta = 0$.

After DM freeze out, so that $y_X^2 \gg (y_X^{\text{eq}} \cdot y_S/y_S^{\text{eq}})^2$, the Boltzmann equation given in Eq. (54) can reduce to

$$\frac{dy_X}{dx} \approx -\frac{1}{x^2} y_X^2. \quad (60)$$

Integrating this approximate equation from the freeze-out epoch $x_f (= m_X/T_f)$ until very late times $x_\infty (\gg x_f)$, one can obtain

$$\frac{1}{y_\infty} - \frac{1}{y_f} = \frac{1}{x_f} - \frac{1}{x_\infty} \quad \Rightarrow \quad y_\infty \simeq x_f, \quad (61)$$

where $y_\infty \ll y_f$. In the following study, along with $\delta = 0$, we use the parameters given in Eq. (48), $m_X = 40$ GeV, $m_S = 35$ GeV, $m_A = 15$ GeV, $g_X = 0.123$, $m_H = m_{H^\pm} = M = 300$ GeV, $\tan \beta = 35$, and $\beta - \alpha = 0.062909$ as a benchmark. The temperature-dependences of g_* and h_{eff} given in Fig. 1 of Ref. [72] are adopted, and their corresponding values, obtained iteratively, at freeze-out temperature are further used in Fig. 7.

Note that there are three different types of relic results which may occur during the dark matter freezes out:

(i) The conventional WIMP dark matter. If the $S \leftrightarrow AA$ and/or $SS \leftrightarrow AA$ interaction(s) are/is strong enough to maintain the chemical equilibrium of the mediator S with the CP-odd Higgs A during the epoch of the dark matter freeze-out, i.e. $y_S = y_S^{\text{eq}}$, then the solution of Eq. (54) is the same as the conventional WIMP dark matter scenario; the corresponding mixing angle θ satisfies $7 \times 10^{-10} < |\theta| < 0.00043$ if taking $\delta = 0$. As an example shown in Fig. 7(a), using $(\theta, \delta) = (0.00043, 0)$, which corresponds to $\lambda_{SAA} \simeq -0.022$, we obtain $x_f = 22$. For the values of $|\lambda_{SAA}| \lesssim 0.022$, we have found that $\langle \sigma v \rangle_{XX \rightarrow AA} / \langle \sigma v \rangle_{XX \rightarrow SS} \lesssim 0.05$, so that the GC gamma-ray excess originating from the two-step cascade annihilation to the final state τ 's is still dominant over the one-step cascade process described by $XX \rightarrow AA$ followed by $A \rightarrow \tau^+ \tau^-$.

(ii) The unconventional WIMP dark matter. If $|\theta|$ is less than 7×10^{-10} but still larger than 2×10^{-10} , the nonrelativistic dark sector particles start to decouple from the thermal bath as for $x \sim 1$. However, for this case, the dark sector can reach again thermal equilibrium with the reservoir before the DM freeze out, so that the dark matter is still WIMP-like, and has the same freeze-out temperature and thermally averaged annihilation cross section as the WIMP case. As an example, using $(\theta, \delta) = (2 \times 10^{-10}, 0)$, which corresponds to $\lambda_{SAA} \simeq -1.03 \times 10^{-8}$, we show the result in Fig. 7(b). See also Fig. 9.

(iii) The co-decaying dark matter. This scenario, for which the corresponding mixing angle is $|\theta| < 2 \times 10^{-10}$ if taking $\delta = 0$, is characterized by $y_S \gg y_S^{\text{eq}}$ and $y_X^2 \gg (y_X^{\text{eq}} \cdot y_S / y_S^{\text{eq}})^2$ at $x = x_f$. For this type of the scenario, featuring by a small $|\lambda_{SAA}| \lesssim 1.03 \times 10^{-8}$, when the dark sector particles become to be nonrelativistic ($x \approx 1$), they start to decouple from the thermal reservoir, and their total yields, $y_X + y_S$, (which is related to the total number density of the dark sector in the co-moving frame) tend to remain constant. Then after a time interval, $\Delta t_\Gamma \approx 2H^{-1}$ (during the radiation dominated epoch) $\sim \Gamma_S^{-1}$, for a degenerate case $m_X \approx m_S$, the dark matter X as well as the mediator S undergoes an exponential decay until freeze-out, of which at the temperature x_f , the Hubble expansion rate H becomes larger than the $XX \rightarrow SS$ annihilation rate. This process is described by the ‘‘co-decaying dark matter’’ mechanism which was proposed by Dror, Kuflik, and Ng [46] for the degenerate case. In the following, we will further discuss a generic case, including the degenerate and non-degenerate ones. We will show that if Δt_Γ is large enough, the exponential suppression for y_X can occur much earlier than y_S due to a significantly suppressed up-scattering rate for the process $SS \rightarrow XX$, such that the DM freeze-out time is earlier than the time that S undergoes an exponential decay. See also Figs. 7(c)-(d).

We then further estimate the value of Δt_Γ for the co-decaying DM. There are two different

cases: (i) $m_X = m_S$, and (ii) $m_X > m_S$. Considering the case of $m_X = m_S$, we sum Eqs. (54) and (59), and neglect the second term of RHS of the latter equation,

$$\frac{d(y_X + y_S)}{dx} \simeq -Cxy_S, \quad (62)$$

with

$$C \equiv \frac{\sqrt{90}}{\pi} M_{\text{pl}} \frac{g_*^{1/2}}{h_{\text{eff}}} \frac{\Gamma_{S \rightarrow AA}}{m_X^2}. \quad (63)$$

Taking the initial conditions: $y_X(1) = y_X^{\text{eq}}(1)$, $y_S(1) = y_S^{\text{eq}}(1)$, and $y_X^{\text{eq}}(1)/y_S^{\text{eq}}(1) = g_X/g_S = 3$, and approximating $y_X + y_S \simeq 4y_S$, we get the solution to Eq. (62),

$$\frac{y_S(x_\Gamma)}{y_S(1)} \simeq e^{-\frac{C}{8}(x_\Gamma^2 - 1)} \stackrel{\text{def}}{=} e^{-1}, \quad (64)$$

with $x_\Gamma \simeq \sqrt{1 + 8/C}$. Because of $\Delta t_\Gamma \simeq (1/2)x_\Gamma^2 C/\Gamma_{S \rightarrow AA}$, this solution can thus be rewritten as

$$\frac{y_S(x_\Gamma)}{y_S(1)} \simeq e^{-\Gamma_{S \rightarrow AA} \Delta t_\Gamma / 4}, \quad (65)$$

for which the lifetime of S is $\Delta t_\Gamma \simeq 4\Gamma_{S \rightarrow AA}^{-1}$. We find that the result shown in Eq. (64) or Eq. (65) can be a good approximation for the case with $x_\Gamma \gtrsim 20$, where the hidden Higgs S can have a sufficient time to satisfy the approximation $y_S - y_S^{\text{eq}} \approx y_S$ which has been taken in Eq. (62).

For the case of $m_X > m_S$, the value of x_Γ depends not only on θ but also on the mass difference of X and S . If the difference of m_X and m_S is sizable enough, then the down-scattering rate, $XX \rightarrow SS$, could be significantly larger than the up-scattering rate, $SS \rightarrow XX$. Under this condition and after a sufficient time with $x_\Gamma \gtrsim 20$, one could have $y_X^{\text{eq}}/y_S^{\text{eq}} \ll 1$ and $y_X \ll y_S$, so that the second and third terms on the right hand side of Eq. (59) are negligible, and this equation can thus be approximated as

$$\frac{dy_S}{dx} \simeq -Cxy_S. \quad (66)$$

From this equation, we get

$$\frac{y_S(x_\Gamma)}{y_S^{\text{in}}(1)} \simeq e^{-\frac{C}{2}(x_\Gamma^2 - 1)} \stackrel{\text{def}}{=} \frac{e^{-1}}{4}, \quad (67)$$

where the effective initial S yield, $y_S^{\text{in}}(1)$, can be approximated as $y_X(1) + y_S(1) \simeq 4y_S(1)$, because the down scattering is larger than the upper one, and the mostly initial X could scatter into S before the S boson undergoes an exponential decay. Therefore, if $m_X - m_S$ is sizable enough, we have $x_\Gamma \simeq \sqrt{1 + 4.8/C}$ and $y_S(x_\Gamma)/y_S(1) \simeq 4e^{-\Gamma_{S \rightarrow AA} \Delta t_\Gamma}$, for which the lifetime of S is $\Delta t_\Gamma \simeq 2.4\Gamma_{S \rightarrow AA}^{-1}$.

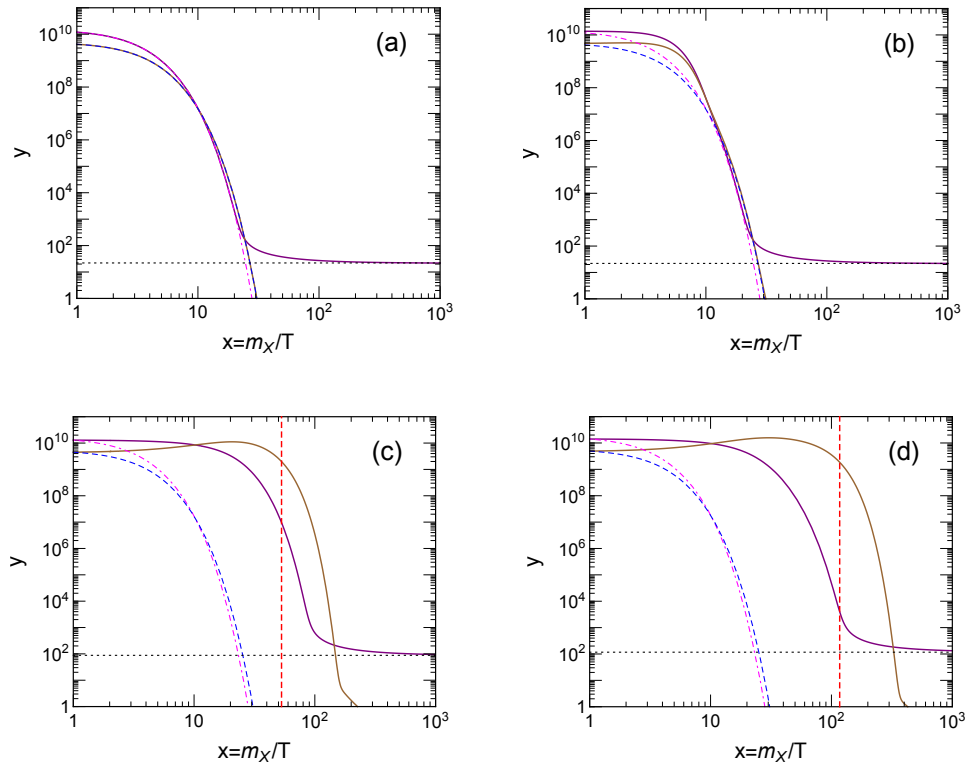


FIG. 7. Evolutions of the dark matter yield y_X and mediator yield y_S , where the parameters given in Eq. (48) are used. The purple solid and brown solid curves stand for y_X and y_S , respectively, while the magenta dashed-dotted and blue dashed curves show their corresponding yields under thermal equilibrium. The horizontal line denotes the asymptotic yield of the dark matter, $y_X^\infty = x_f$. In (a), (b), (c), and (d), we separately use $(\theta, \delta) = (0.00043, 0), (2 \times 10^{-10}, 0), (1.2 \times 10^{-11}, 0)$, and $(5.1 \times 10^{-12}, 0)$ as inputs, for which the resulting λ_{SAA} are $-0.022, -1.03 \times 10^{-8}, -6.16 \times 10^{-10}$ and -2.62×10^{-10} , and the corresponding x_f are 22, 22, 88, and 117, respectively. The vertical dashed (red) lines in (c) and (d) indicate the values of x_Γ obtained by Eq. (67).

In general, for a co-decay process with $x_\Gamma \gtrsim 20$, we get $\sqrt{1 + 4.8/C} \lesssim x_\Gamma \lesssim \sqrt{1 + 8/C}$. Taking the same parameters which have been used, but adopting m_S as a free parameter, we find that $x_\Gamma = \sqrt{1 + 4.8/C}$ is a good approximation provided that $2m_A < m_S \lesssim 35$ GeV. Figs. 7(c) and (d) show the values of x_Γ to be about 51 and 117, respectively, where the latter satisfies $x_\Gamma \approx x_f$. For a process with a much larger x_Γ as shown in Figs. 7(c) and (d), the inequality $y_S > y_X$, i.e. $n_S > n_X$, becomes much more noticeable and, due to a suppressed up-scattering rate, the exponential suppression for n_X occurs much earlier than n_S .

2. Including the cannibal interactions, $XXS \leftrightarrow SS$, $SSS \leftrightarrow XX$, $SSS \leftrightarrow SS$ and $XSS \leftrightarrow XS$, in the coupled Boltzmann equations: a more complete treatment

It was stressed in Refs. [47, 48] that when the hidden sector is out of the thermal equilibrium with the bath, the hidden particles may undergo so-called cannibalism before DM freeze-out. Here we include the cannibal interactions, $XXS \leftrightarrow SS$, $SSS \leftrightarrow XX$, $SSS \leftrightarrow SS$ and $XSS \leftrightarrow XS$, which are number changing annihilations, in the Boltzmann equations,

$$\frac{dn_X}{dt} + 3Hn_X = \dots - \langle \sigma v^2 \rangle_{XXS \rightarrow SS} \left[n_X^2 n_S - (n_X^{\text{eq}})^2 \frac{n_S^2}{(n_S^{\text{eq}})^2} \right] + \frac{1}{3} \langle \sigma v^2 \rangle_{SSS \rightarrow XX} \left[n_S^3 - (n_S^{\text{eq}})^3 \frac{n_X^2}{(n_X^{\text{eq}})^2} \right], \quad (68)$$

$$\begin{aligned} \frac{dn_S}{dt} + 3Hn_S = \dots &- \frac{1}{6} \langle \sigma v^2 \rangle_{SSS \rightarrow SS} \left[n_S^3 - n_S^2 n_S^{\text{eq}} \right] - \frac{1}{2} \langle \sigma v^2 \rangle_{XSS \rightarrow XS} \left[n_X n_S^2 - n_X n_S n_S^{\text{eq}} \right] \\ &+ \frac{1}{2} \langle \sigma v^2 \rangle_{XXS \rightarrow SS} \left[n_X^2 n_S - (n_X^{\text{eq}})^2 \frac{n_S^2}{(n_S^{\text{eq}})^2} \right] - \frac{1}{2} \langle \sigma v^2 \rangle_{SSS \rightarrow XX} \left[n_S^3 - (n_S^{\text{eq}})^3 \frac{n_X^2}{(n_X^{\text{eq}})^2} \right], \end{aligned} \quad (69)$$

where the dots are all terms of the right hand side of Eqs. (50) and (51), respectively, and $\langle \sigma v^2 \rangle$ is the thermally averaged annihilation cross section for the $3 \rightarrow 2$ cannibal process. One can refer to Ref. [75] for a general form of $3 \rightarrow 2$ scattering rates. In each cannibal term of the above equations, the factor (including the relative sign) in front of the cross section equals to $\Delta n_i / N!$, where $1/N!$ is for avoiding the double counting for the initial number density in the reaction with N being the number of the identical particles of the initial states for the relevant cross section, and Δn_i is the number change for the hidden particle with $i \equiv X$ for Eq. (50) or $\equiv S$ for (51); for instance, for the process $SSS \rightarrow XX$, we have $N = 3$, but $\Delta n_X = 2$, $\Delta n_S = -3$, resulting in the factor $1/3$ and $-1/2$ shown in the corresponding terms in Eqs. (68) and (69), respectively.

To calculate $3 \rightarrow 2$ thermally averaged annihilation cross sections for the nonrelativistic dark sector particles with $x \lesssim 1$, we take the low-velocity approximation, $\langle \sigma v^2 \rangle \simeq \sigma v^2$, by neglecting the correction of $\mathcal{O}(T/m_X)$:

$$\langle \sigma v^2 \rangle_{XXS \rightarrow SS} \simeq \frac{[(2m_X - m_S)(2m_X + 3m_S)]^{1/2}}{128\pi m_X^4 m_S (2m_X + m_S)} g_X^6 \frac{96275}{5184} \left(1 - \frac{4.33\delta}{m_X} + \frac{5.25\delta^2}{m_X^2} - \frac{0.68\delta^3}{m_X^3} \right), \quad (70)$$

$$\langle \sigma v^2 \rangle_{SSS \rightarrow XX} \simeq \frac{\sqrt{9 - 4m_X^2/m_S^2}}{384\pi m_S^3 m_X^2} g_X^6 \frac{1377}{16} \left(1 + \frac{7.76\delta}{m_X} + \frac{18.3\delta^2}{m_X^2} - \frac{42.3\delta^3}{m_X^3} \right), \quad (71)$$

$$\langle \sigma v^2 \rangle_{SSS \rightarrow SS} \simeq \frac{\sqrt{5}}{384\pi} \frac{18225}{16m_S^5} \left(\frac{g_X m_S}{m_X} \right)^6, \quad (72)$$

$$\langle \sigma v^2 \rangle_{XSS \rightarrow XS} \simeq \frac{[3(2m_X + m_S)(2m_X + 3m_S)]^{1/2}}{128\pi m_X^3 m_S (m_X + 2m_S)^2} g_X^6 \frac{21425}{54} \left(1 - \frac{2.89\delta}{m_X} + \frac{3.08\delta^2}{m_X^2} - \frac{1.56\delta^3}{m_X^3} \right), \quad (73)$$

with $\delta \equiv m_X - m_S$. Here, because the expressions of $XXS \leftrightarrow SS$, $SSS \leftrightarrow XX$, and $XSS \leftrightarrow XS$ are lengthy, with good approximations we thus expand their amplitudes squared up to $\mathcal{O}(\delta^3/m_X^3)$.

Again, we further rewrite Eqs. (68) and (69) as

$$\begin{aligned} \frac{dy_X}{dx} = \dots &+ \frac{\pi}{\sqrt{90}} \frac{h_{\text{eff}}}{g_*^{1/2}} \frac{m_X^2}{M_{\text{pl}}} \frac{1}{x^5} \left[- \frac{\langle \sigma v^2 \rangle_{XXS \rightarrow SS}}{(\langle \sigma v \rangle_{XX \rightarrow SS})^2} \left(y_X^2 y_S - \frac{y_S^2}{y_S^{\text{eq}}} (y_X^{\text{eq}})^2 \right) \right. \\ &\left. + \frac{1}{3} \frac{\langle \sigma v^2 \rangle_{SSS \rightarrow XX}}{(\langle \sigma v \rangle_{XX \rightarrow SS})^2} \left(y_S^3 - \frac{y_X^2}{(y_X^{\text{eq}})^2} (y_S^{\text{eq}})^3 \right) \right], \end{aligned} \quad (74)$$

$$\begin{aligned} \frac{dy_S}{dx} = \dots &+ \frac{\pi}{\sqrt{90}} \frac{h_{\text{eff}}}{g_*^{1/2}} \frac{m_X^2}{M_{\text{pl}}} \frac{1}{x^5} \left[- \frac{1}{6} \frac{\langle \sigma v^2 \rangle_{SSS \rightarrow SS}}{(\langle \sigma v \rangle_{XX \rightarrow SS})^2} \left(y_S^3 - y_S^2 y_S^{\text{eq}} \right) \right. \\ &- \frac{1}{2} \frac{\langle \sigma v^2 \rangle_{XSS \rightarrow XS}}{(\langle \sigma v \rangle_{XX \rightarrow SS})^2} \left(y_X y_S^2 - y_X y_S y_S^{\text{eq}} \right) + \frac{1}{2} \frac{\langle \sigma v^2 \rangle_{XXS \rightarrow SS}}{(\langle \sigma v \rangle_{XX \rightarrow SS})^2} \left(y_X^2 y_S - \frac{y_S^2}{y_S^{\text{eq}}} (y_X^{\text{eq}})^2 \right) \\ &\left. - \frac{1}{2} \frac{\langle \sigma v^2 \rangle_{SSS \rightarrow XX}}{(\langle \sigma v \rangle_{XX \rightarrow SS})^2} \left(y_S^3 - \frac{y_X^2}{(y_X^{\text{eq}})^2} (y_S^{\text{eq}})^3 \right) \right], \end{aligned} \quad (75)$$

where the value of $\langle \sigma v \rangle_{XX \rightarrow SS}$ used in the numerical analysis satisfies Eqs. (76) and (77).

As shown in Fig. 7(b), (c) and (d), for the case of $|\theta| < 7 \times 10^{-10}$, when $x \lesssim 1$, the dark sector particles become nonrelativistic and are kinetically decoupled from the thermal bath due to small $S \leftrightarrow AA$ and $SS \leftrightarrow AA$ interaction rates, so that the comoving number density of the total hidden sector particles remain constant before the time that the hidden Higgs bosons undergo the exponential decay. However, in the present case, the cannibal annihilations cannot be neglected. We take Eq. (68) as an example to give a qualitative analysis on cannibalization as follows. The left hand side is of order $n_X H$, while the right hand side due to $XXS \rightarrow SS$ is of order $n_X^2 n_S \langle \sigma v^2 \rangle_{XXS \rightarrow SS}$. Therefore, if the $XXS \rightarrow SS$ reaction rate is much larger than the expansion rate, the only way to maintain the equality of Eq. (68) is to have $n_X = n_X^{\text{eq}}$ and $n_S = n_S^{\text{eq}}$, about which one can obtain the same conclusion using either $SSS \rightarrow XX$, $SSS \rightarrow SS$, $XSS \rightarrow XS$, or Eq. (68) in doing a similar analysis.

Using the same parameters as in Sec. VB1, and further including the $3 \leftrightarrow 2$ interactions in the Boltzmann equations, in Fig. 8 we show the results of the normalized yields. Compared with Fig. 7(c) and (d), at x_Γ , which has been obtained in Eq. (67), the corresponding value of y_S (and also the number density of S) reduces 2 orders of magnitude due to the cannibal effect. Fig. 8(c) and (d) are typical examples about the cannibally co-decaying DM, where, at $x = x_{\text{can}} \approx 7$, the cannibal annihilation rate becomes less than the expansion rate of the Universe, so that the number densities of X and S no longer track up the behavior of the Boltzmann suppression. The resulting $x_f = 70$ for Fig. 8(c) and 97 for (d) are significantly smaller than that with the cannibal interactions neglected.

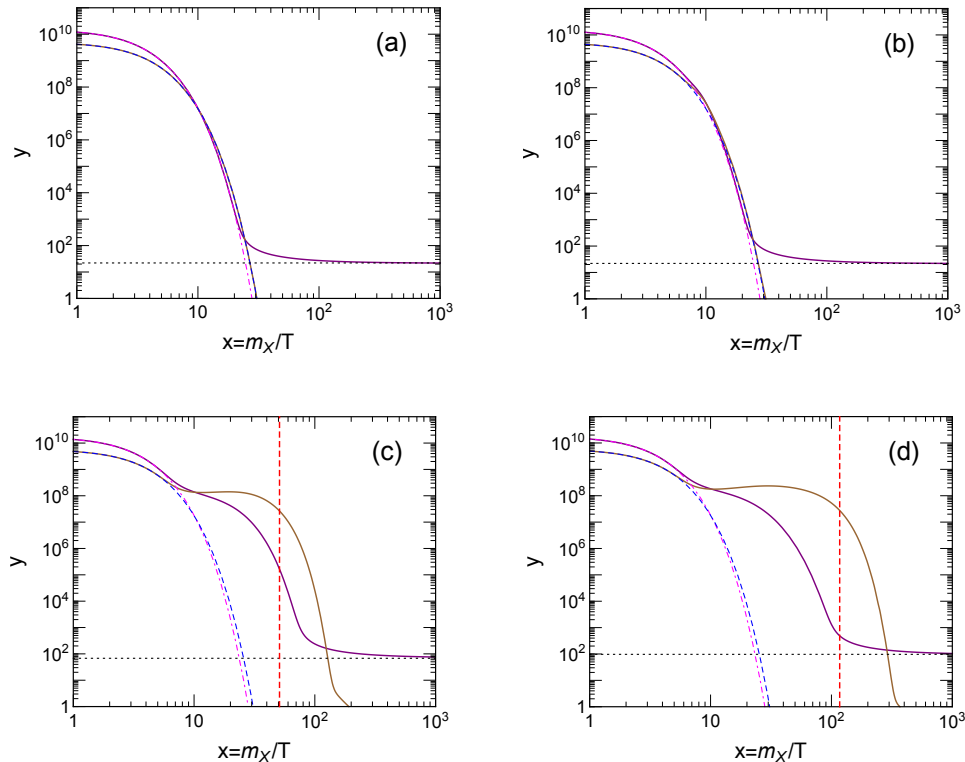


FIG. 8. Same as Fig. 7 but the $3 \leftrightarrow 2$ interactions are included in the Boltzmann equations. In (a) and (b), the resulting x_f is still to be 22, whereas in (c) and (d), the values of x_f are 70 and 97, respectively. We show the same corresponding x_Γ as Fig. 7, for which the value is 51 in (c) and 117 in (d).

In concluding this section, we would like to discuss the relations and constraints between the parameters and observables. The $XX \rightarrow SS$ annihilation cross section and x_f can be related to each other via the DM relic abundance. The dimensionless density parameter of the present-day DM relic abundance, determined to be $\Omega_{\text{DM}} = (0.1198 \pm 0.0026)/h^2$ from the observations [73, 76], is given by [71]

$$\Omega_{\text{DM}} = \frac{m_X n_X}{\rho_c} = \frac{Y_X^\infty s_0 m_X}{\rho_c} \simeq \frac{1.04 \times 10^9 \text{ GeV}^{-1}}{J \sqrt{8\pi g_* M_{\text{pl}} h^2}}, \quad (76)$$

where Y_X^∞ , related to y_X^∞ via Eq. (52), is the post-freeze-out value of Y_X , $\rho_c = 3H_0^2/(8\pi G)$ is the present critical density, $h \simeq 0.678$ is the present-day Hubble constant H_0 in units of $100 \text{ km s}^{-1} \text{ Mpc}^{-1}$, $s_0 = 2891 \text{ cm}^{-3}$ is the present-day entropy, and

$$J = \int_{x_f}^{\infty} \frac{\langle \sigma v \rangle_{XX \rightarrow SS}}{x^2} dx \approx \frac{\langle \sigma v \rangle_{XX \rightarrow SS}^{(0)}}{x_f}. \quad (77)$$

In Fig. 9, we show x_f as a function of θ , where the relations between x_f and the $XX \rightarrow SS$ annihilation cross section $\langle \sigma v \rangle$, and between θ and $\Gamma(S \rightarrow AA)$ are depicted. For simplicity, we

have approximated the thermally averaged DM annihilation cross section by using its leading s -wave value in $v \rightarrow 0$ limit. Note that the vertical axis for the annihilation cross section has been rescaled by use of the temperature-dependent g_* given in Ref. [72]. Moreover, in this lepton-specific (type-X) N2HDM portal vector dark matter model, the total width of S satisfies $\Gamma_S \simeq \Gamma(S \rightarrow AA)$ with taking $\delta = 0$.

In Fig. 9, if θ is less than 0.00043, denoted by the vertical dotted (blue) line, the GC gamma-ray annihilation is dominated by the 2-step cascade DM annihilation. For $\theta \lesssim 7 \times 10^{-10}$, corresponding to the left hand side of the right dashed (red) line, the dark sector decouples from the thermal reservoir when $x \approx 1$. However, within the range $2 \times 10^{-10} \lesssim \theta \lesssim 7 \times 10^{-10}$, i.e. $-1.03 \times 10^{-8} \gtrsim \lambda_{SAA} \gtrsim -3.60 \times 10^{-8}$, which is in between the two vertical dashed (red) lines, due to the co-decay and cannibal annihilation of the dark sector, the re-thermalized dark sector can be again in thermal equilibrium with the thermal reservoir before the DM freeze out; see also Fig. 7(b) and Fig. 8(b).

For a case with a large value of x_Γ , the normalized yield y_S does not tend to decay exponentially until the time $t \sim t_\Gamma$. Due to a significantly suppressed up-scattering rate, the exponential suppression for y_X can occur much earlier than that for y_S . Moreover, the cannibal annihilations also reduce the value of x_f . Therefore, as shown in Fig. 8(d), we can have $x_\Gamma \gtrsim x_f$. In Fig. 9, for $\theta < 7.5 \times 10^{-12}$ denoted by vertical solid (magenta) line, we have $x_\Gamma > x_f$. It should be noted that the approximation for the temperature dependence of DoF given in Ref. [72] breaks down during the QCD phase transition which may occur in the temperature range of 150 – 400 MeV, i.e. corresponding to $x \sim 100 - 267$ for $m_X = 40$ GeV. For simplicity, the freeze-out results shown in Figs. 7(d) and 9 are assumed to occur before the QCD phase transition.

We then further discuss the big bang nucleosynthesis (BBN) and cosmic microwave background (CMB) constraints. The requirement of avoiding the n/p ratio and ${}^4\text{He}$ abundance to deviate from the standard BBN [77] is to have $\Gamma_S^{-1} \lesssim 1$ sec, which imposes a quite relaxed bound of $|\lambda_{SAA}| \gtrsim 2.7 \times 10^{-13}$, $|\theta| \gtrsim 5.3 \times 10^{-15}$ with taking $\delta = 0$. As for the Planck result for the CMB [78] which provides a probe of the DM annihilation at the time of recombination, $t_{\text{CMB}} \sim 380,000$ yrs, the resulting bound is highly insensitively dependent on the number of cascade steps (see Fig. 11 of Ref. [42]), and gives $\langle \sigma v \rangle \lesssim (7 - 19) \times 10^{-26}$ cm³/s. The current CMB constraint is modestly weaker than that given by the observations of dSphs.

Note that by varying the local dark matter density from 0.357 GeV/cm³ to 0.2 GeV/cm³ and the halo slope γ from 1.2 to 1.1, the annihilation cross section allowed by the GC data fit, shown in Fig. 4, would be further extended by a factor of ~ 4.10 upward. In Fig. 9, the horizontal dot-dashed (purple) line depicts the 95% C.L. upper limit on the annihilation cross

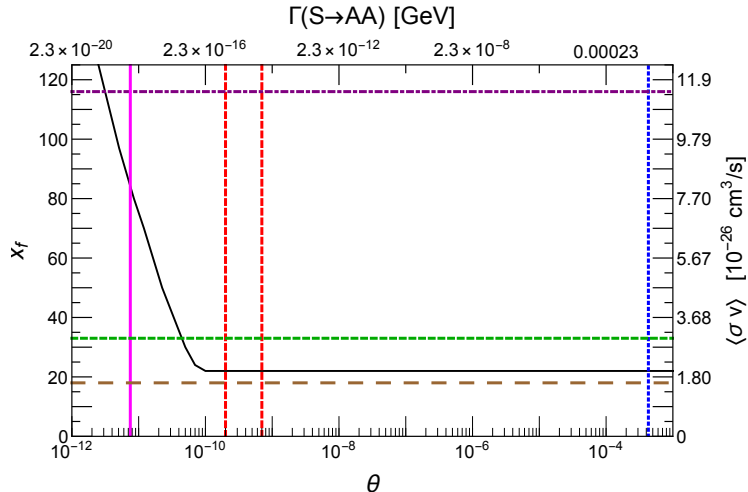


FIG. 9. x_f (or the $XX \rightarrow SS$ annihilation cross section $\langle\sigma v\rangle$) as a function of θ (or $\Gamma(S \rightarrow AA)$), denoted as the black curve to show the relic result, where we have adopted $\delta = 0$ and the parameters given in Eq. (48). When the θ is smaller than that denoted by the vertical dotted (blue) line, the GC gamma-ray excess is dominated by the 2-step cascade annihilation. For a θ smaller than that denoted by right dashed (red) line, the dark sector decouples from the thermal bath when $x \lesssim 1$. The range of θ between the two vertical dashed (red) lines denotes that the DM X as well as the mediator S can be again in thermal equilibrium with the thermal bath before freeze out. The horizontal dot-dashed (purple) line shows the maximum value of the annihilation cross section that could still account for the GC gamma-ray excess. The 95% C.L. upper limit and project sensitivity for observation of dSphs are denoted as horizontal dashed (green) and long-dashed (brown) lines, respectively. For a θ smaller than that denoted by the vertical solid (magenta) line, we have $x_\Gamma > x_f$.

section ($\langle\sigma v\rangle \simeq 1.15 \times 10^{-25} \text{ cm}^3/\text{s}$), corresponding to $x_f \simeq 116$, to account for the GC gamma-ray excess due to variations of ρ_\odot and γ . In Fig. 9, we also show the current constraint from the observations of the dSphs, and the projected sensitivity for observations of 60 dSphs with 15-year data collection. The dSph projected limit on $\langle\sigma v\rangle$ is likely to be improved by a factor of ~ 1.83 .

VI. DISCUSSIONS AND CONCLUSIONS

Before making conclusion, we would like to discuss the parameter space in favor of the measurement of the muon anomalous magnetic moment $a_\mu \equiv (g - 2)/2$ [73, 79], which can especially constrain the parameters, m_A and $\tan\beta$. The discrepancy between the experiments and SM pre-

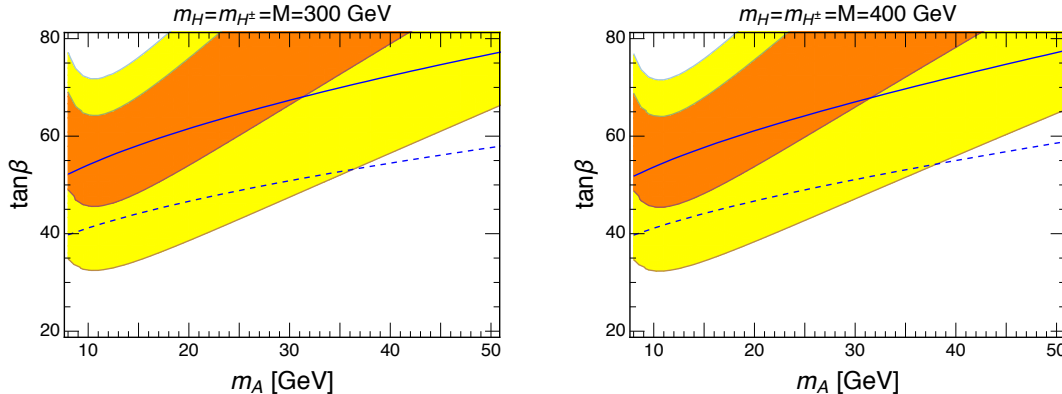


FIG. 10. The $g - 2$ allowed regions with 1σ C.L. (orange) and 2σ C.L. (yellow) on the m_A - $\tan\beta$ plane vs. 95% C.L. and 99% C.L. upper limits denoted as the dashed and solid blue lines, respectively, from the lepton universality and τ decay constraints.

diction is more than 3σ confidence level [80, 81]:

$$a_\mu^{\text{exp}} - a_\mu^{\text{SM}} = (262 \pm 86) \times 10^{-11}. \quad (78)$$

In this secluded DM model, the mixing angles between the hidden Higgs boson and the visible two-Higgs doublets are very small, such that the dominant contributions to a_μ are from the visible sectors. It was shown in Ref. [82] that the two-loop Barr-Zee diagrams can give sizable contributions to a_μ . For our model, in contrast with the one-loop result, the two-loop diagram containing an A propagator with m_A being $\mathcal{O}(10)$ GeV gives positive contributions to a_μ and its magnitude is even larger than that of one-loop. We collect the relevant a_μ calculations in the lepton-specific N2HDM in Appendix E 1.

In Fig. 10, we show the $g - 2$ allowed regions at 1σ C.L. and 2σ C.L. on the m_A - $\tan\beta$ plane vs. 95% C.L. and 99% C.L. upper limits from the lepton universality and τ decays, where we impose $\lambda_{hAA} = 0$ to have $\text{Br}(h \rightarrow AA) = 0$, and then show the results for two different values of $\sqrt{M^2} = m_H = m_{H^\pm} = 300$ and 400 GeV. A larger m_H can suppress the negative two-loop correction, whereas the output seems to be insensitive to variation of its value. We also take $m_S = 35$ GeV as input. However, because the result is insensitive to the values of the θ and δ due to their smallness, the hidden Higgs boson is secluded from the SM related phenomenology, just as the present case; thus the $g - 2$ result that we have shown here is basically consistent with that in the type-X 2HDM. The τ decays and lepton universality, which was stressed in Ref. [44], can provide a stringent bound on parameter space favored by $g - 2$. The relevant formulas and data are summarized in Appendix E 2. As shown in Fig. 10, the result, capable of accounting for the muon

$g - 2$ anomaly at the 2σ level but without violating the constraint from the lepton universality and τ decays at 95% C.L., favors the parameter space in which $8 \lesssim m_A \lesssim 37$ GeV and $30 \lesssim \tan \beta \lesssim 55$ for $m_H \sim 300\text{-}400$ GeV.

It is interesting to note that the $B_s \rightarrow \mu^+ \mu^-$ data disfavor $m_A \lesssim 10$ GeV for $m_H = m_{H^\pm} = 300$ GeV, but the constraint is less restrictive for larger m_H and m_{H^\pm} [44]. Moreover, a precise measurement can also provide a stringent constraint on m_A and M^2 (see Eq. (33) for reference).

We give our conclusion as follows. We have built a hidden sector dark matter model with dark discrete Z_2 symmetry which is the remnant of the spontaneously broken dark $U(1)_{\text{dm}}$ gauge group. After symmetry breaking, the hidden sector contains vector dark matter, along with a real hidden Higgs mediating the DM interactions to the visible sector through the mixing among the neutral Higgs bosons in the model, while the visible sector is the lepton-specific 2HDM.

In this model, the GC gamma-ray excess is mainly due to the 2-step cascade annihilation describing that the vector dark matter particles annihilate to the pairs of hidden scalars, S , which subsequently undergo the decays $S \rightarrow AA$ and then $A \rightarrow \tau^- \tau^+$. We find the parameter space with $m_X \sim 25 - 50$ GeV, $m_A \sim 3.6 - 25$ GeV, and $m_X \gtrsim m_S \gtrsim 2m_A$ can provide a good fit to the GC gamma-ray excess spectrum. The obtained mass of the CP-odd Higgs A in the GC excess fit can explain the muon $g - 2$ anomaly at the 2σ level without violating the stringent constraints from the lepton universality and τ decays.

Provided that the GC gamma-ray excess is generated by the 2-step cascade annihilation, the interplay of the hidden sector and visible sector mainly arises from the interaction $S \leftrightarrow AA$ which is dominant over $SS \leftrightarrow AA$, where the interaction coupling depends on the mixing angles between the hidden Higgs boson and visible ones. We have shown that three different freeze-out types for the DM relic abundance, depending on such mixing angles, may occur, and correspond to the magnitudes of coupling constant λ_{SAA} to be (i) in between 3.60×10^{-8} and 0.022, (ii) in between 1.03×10^{-8} and 3.60×10^{-8} , and (iii) less than 1.03×10^{-8} .

For the type (i), the hidden Higgs (mediator) can be in chemical and thermal equilibrium with the bath, and the DM particles, consistent the thermal WIMP scenario, are Boltzmann suppressed until freeze out. For the type (ii), when the temperature of the thermal bath decreases with $T \lesssim m_X, m_S$, the nonrelativistic particles in the dark sector decouple from the bath. Nevertheless, the dark sector can be again in thermal equilibrium with the bath before freeze out, so that the dark matter particles behave like WIMPs finally. See Figs. 8(b) and 9 for example. For the type (iii) which is a typical case of the cannibally co-decaying DM, the dark sector decouples from the thermal background at the temperature below their masses, but undergoes a cannibal phase first.

After that, the total comoving number density of the dark sector will not exponentially suppressed until the time that the mediator decaying to the CP-odd Higgs boson pair occurs. For this type, the exponential suppression for the comoving dark matter number density could occur much earlier than that for the mediator due to a significantly kinematical suppression on the up-scattering ($SS \rightarrow XX$) rate. See Sec. VB for details.

The vector dark matter in the hidden sector does not directly couple to the visible sector¹, but instead annihilates into the “short-lived” hidden Higgs bosons which decay through a small coupling into the CP-odd Higgs bosons. Considering the BBN bound, the lifetime of the short-lived hidden Higgs is required to be less than 1 sec, which imposes a quite relaxed constraint on the coupling $|\lambda_{SAA}| \gtrsim 2.7 \times 10^{-13}$. Therefore, due to the very small coupling constant, $|\lambda_{SAA}| < 0.022$, the DM in the hidden sector is secluded from detections in the direct searches or colliders even though the resultant DM annihilation cross section in the case of type (iii) could be much larger than that in the thermal WIMP scenario, as shown in Fig. 9.

However, the DM annihilation signals are not suppressed in a general hidden sector model. We have shown the constraints from the observations of dSphs and from the 15-year Fermi-LAT projected sensitivity of 60 dSphs, where the projected limit on $\langle\sigma v\rangle$ might be improved by a factor of ~ 1.83 . The observations of dSphs thus provide a promising way to test this hidden dark matter model in the near future.

ACKNOWLEDGMENTS

I would like to thank Joshua T. Ruderman for helpful correspondence. This work was supported in part by the Ministry of Science and Technology, Taiwan, under Grant No. 105-2112-M-033-005.

Appendix A: Theoretical constraints

The parameters in the Type-X N2HDM scalar potential are subjected to the following theoretical constraints.

Perturbativity

To make sure the validity of the perturbative expansion, we impose the couplings to satisfy

$$g_X^2 < 4\pi, \quad |\lambda_i| < 4\pi, \quad \text{for } i = 1, \dots, 8. \quad (\text{A1})$$

¹ Precisely speaking, the dark matter can couple to the visible sector via the (visible) Higgs bosons, but, due to the negligibly small coupling constants, such contributions are highly suppressed.

Vacuum stability

To have a potential bounded from below, the allowed parameter regions satisfy the conditions [83, 84],

$$\left(\lambda_1, \lambda_2, \lambda_6 > 0, \sqrt{\lambda_1 \lambda_6} + \lambda_7 > 0, \sqrt{\lambda_2 \lambda_6} + \lambda_8 > 0, \sqrt{\lambda_1 \lambda_2} + \lambda_3 + D > 0, \lambda_7 + \sqrt{\frac{\lambda_1}{\lambda_2}} \lambda_8 \geq 0 \right)$$

or

$$\left(\lambda_1, \lambda_2, \lambda_6 > 0, \sqrt{\lambda_2 \lambda_6} \geq \lambda_8 > -\sqrt{\lambda_2 \lambda_6}, \sqrt{\lambda_1 \lambda_6} > -\lambda_7 \geq \sqrt{\frac{\lambda_1}{\lambda_2}} \lambda_8, \sqrt{(\lambda_7^2 - \lambda_1 \lambda_6)(\lambda_8^2 - \lambda_2 \lambda_6)} > \lambda_7 \lambda_8 - (D + \lambda_3) \lambda_6 \right), \quad (\text{A2})$$

with

$$D = \begin{cases} \lambda_4 - \lambda_5 & \text{for } \lambda_4 > \lambda_5 \\ 0 & \text{for } \lambda_4 \leq \lambda_5 \end{cases}. \quad (\text{A3})$$

Tree-level perturbative unitarity

The tree-level perturbative unitarity is obtained by requiring that all absolute eigenvalues of the two-body scalar scattering matrix are less than 8π . The constraints are given by [83–85]

$$|\lambda_3 - \lambda_4| < 8\pi, \quad (\text{A4})$$

$$|\lambda_3 + 2\lambda_4 \pm 3\lambda_5| < 8\pi, \quad (\text{A5})$$

$$\left| \frac{1}{2} \left(\lambda_1 + \lambda_2 + \sqrt{(\lambda_1 - \lambda_2)^2 + 4\lambda_4^2} \right) \right| < 8\pi, \quad (\text{A6})$$

$$\left| \frac{1}{2} \left(\lambda_1 + \lambda_2 + \sqrt{(\lambda_1 - \lambda_2)^2 + 4\lambda_5^2} \right) \right| < 8\pi, \quad (\text{A7})$$

$$|a_{1,2,3}| < 8\pi, \quad (\text{A8})$$

where $a_{1,2,3}$ are the real roots of the following equation,

$$\begin{aligned} & 4(-27\lambda_1\lambda_2\lambda_6 + 12\lambda_3^2\lambda_6 + 12\lambda_3\lambda_4\lambda_6 + 3\lambda_4^2\lambda_6 + 6\lambda_2\lambda_7^2 - 8\lambda_3\lambda_7\lambda_8 - 4\lambda_4\lambda_7\lambda_8 + 6\lambda_1\lambda_8^2) \\ & + x(36\lambda_1\lambda_2 - 16\lambda_3^2 - 16\lambda_3\lambda_4 - 4\lambda_4^2 + 18\lambda_1\lambda_6 + 18\lambda_2\lambda_6 - 4\lambda_7^2 - 4\lambda_8^2) \\ & + x^2(-6(\lambda_1 + \lambda_2) - 3\lambda_6) + x^3 = 0. \end{aligned} \quad (\text{A9})$$

Appendix B: The quartic couplings in the Higgs potential of the next-to-minimal two-Higgs doublet portal vector DM model

Keeping terms linear in $\sin \theta$ and $\sin \delta$, the quartic couplings λ_i can be expressed in terms of M and the physical Higgs masses as

$$\lambda_1 \simeq \frac{1}{v^2 c_\beta^2} (-M^2 s_\beta^2 + m_h^2 s_\alpha^2 + m_H^2 c_\alpha^2), \quad (\text{B1})$$

$$\lambda_2 \simeq \frac{1}{v^2 s_\beta^2} (-M^2 c_\beta^2 + m_h^2 c_\alpha^2 + m_H^2 s_\alpha^2), \quad (\text{B2})$$

$$\lambda_3 \simeq \frac{1}{v^2} \left[-M^2 + 2m_{H^\pm}^2 + \frac{1}{s_\beta^2 c_\beta^2} (-m_h^2 s_\alpha c_\alpha + m_H^2 s_\alpha c_\alpha) \right], \quad (\text{B3})$$

$$\lambda_4 \simeq \frac{1}{v^2} (M^2 - m_A^2 - 2m_{H^\pm}^2), \quad (\text{B4})$$

$$\lambda_5 \simeq \frac{1}{v^2} (M^2 - m_A^2), \quad (\text{B5})$$

$$\lambda_6 \simeq \frac{m_S^2}{v_S^2}, \quad (\text{B6})$$

$$\lambda_7 \simeq \frac{1}{vv_S c_\beta} (m_H^2 c_\alpha s_\theta - m_h^2 s_\alpha s_\delta - m_S^2 (c_\alpha s_\theta - s_\alpha s_\delta)), \quad (\text{B7})$$

$$\lambda_8 \simeq \frac{1}{vv_S s_\beta} (m_H^2 s_\alpha s_\theta + m_h^2 c_\alpha s_\delta - m_S^2 (s_\alpha s_\theta + c_\alpha s_\delta)). \quad (\text{B8})$$

Appendix C: Oblique parameters

The new physics effects can contribute to the gauge boson vacuum polarization amplitudes, and can be described by the three oblique parameters, S, T and U at the one-loop level. We adopt the definition of these parameters, which were originally introduced by Peskin and Takeuchi (PT) and expanded to the linear order in q^2 [56, 57]. Considering the expansion beyond linear order, the new physics effects, introduced by Maksymyk, Burgess and London (MBL) [86], were defined as 6 parameters, S, T, U, V, W and X . The PT parameters can be related to the MBL ones as $S_{\text{PT}} = S_{\text{MBL}} + 4(c_w^2 - s_w^2)X_{\text{MBL}}$, $T_{\text{PT}} = T_{\text{MBL}}$, and $U_{\text{PT}} = U_{\text{MBL}} + 8s_w^2 X_{\text{MBL}}$ [87], where $s_w \equiv \sin \theta_W = 0.23129$ and $c_w \equiv \cos \theta_W$ at the scale $\mu = m_Z$. Taking the limit $s_{\beta-\alpha} \rightarrow 1$, and keeping terms linear in $\sin \theta$ and $\sin \delta$, we obtain the three PT parameters in the present model from a general multi-Higgs-doublet study in the MBL formulas given in Ref. [58], and express the

approximate result as

$$T \simeq \frac{1}{16\pi^2\alpha_{\text{em}}v^2} (F(m_{H^\pm}^2, m_H^2) + F(m_{H^\pm}^2, m_A^2) - F(m_H^2, m_A^2)), \quad (\text{C1})$$

$$S \simeq \frac{1}{24\pi} \left(G(m_H^2, m_A^2, m_Z^2) - (2s_w^2 - 1)^2 G(m_{H^\pm}^2, m_{H^\pm}^2, m_Z^2) + \ln \left(\frac{m_H^2 m_A^2}{m_{H^\pm}^4} \right) \right), \quad (\text{C2})$$

$$U \simeq \frac{1}{24\pi} (G(m_{H^\pm}^2, m_H^2, m_W^2) + G(m_{H^\pm}^2, m_A^2, m_W^2) - G(m_H^2, m_A^2, m_Z^2) \\ + (4s_w^4 - 1)G(m_{H^\pm}^2, m_{H^\pm}^2, m_Z^2)), \quad (\text{C3})$$

where $\alpha_{\text{em}} = 1/127.950$ at the scale m_Z , the function F is given by

$$F(m_1^2, m_2^2) = \begin{cases} \frac{m_1^2 + m_2^2}{2} - \frac{m_1^2 m_2^2}{m_1^2 - m_2^2} \ln \frac{m_1^2}{m_2^2}, & \text{for } m_1^2 \neq m_2^2, \\ 0, & \text{for } m_1^2 = m_2^2, \end{cases} \quad (\text{C4})$$

and the function G , which is in a more complicated form, can be referred to Ref. [58]. In the limit $|m_{H^\pm} - m_H| \ll m_H$, $m_A \ll m_H$, the oblique parameters can be further approximated as

$$T \approx \frac{1}{32\pi^2\alpha_{\text{em}}v^2} m_H (m_{H^\pm} - m_H), \\ S \approx -\frac{1}{24\pi} \left(\frac{5}{3} + \frac{1}{2} \frac{m_Z^2}{m_H^2} - \frac{(2s_w^2 - 1)^2}{5} \frac{m_Z^2}{m_{H^\pm}^2} + \frac{4(m_{H^\pm} - m_H)}{m_H} \right), \\ U \approx \frac{1}{12\pi} \left[-\frac{1}{10} \frac{m_W^2}{m_{H^\pm}^2} \left(1 + \frac{4s_w^4 - 1}{c_w^2} \right) + \frac{1}{4} m_Z^2 \frac{m_{H^\pm}^2 - c_w^2 m_H^2}{m_H^2 m_{H^\pm}^2} + \frac{m_{H^\pm} - m_H}{m_H} \right]. \quad (\text{C5})$$

Appendix D: Annihilation cross sections

1. The annihilation process $XX \rightarrow SS$

The DM annihilation processes for $XX \rightarrow SS$, relevant to the calculations of the thermal relic abundance and indirect measurements, are shown in Fig. 2, and their cross sections can be expressed as

$$\sigma v_{\text{lab}} = (\sigma v_{\text{lab}})_{4\nu, s} + (\sigma v_{\text{lab}})_{t, u} + (\sigma v_{\text{lab}})_{\text{int}}, \quad (\text{D1})$$

where $(\sigma v_{\text{lab}})_{4v,s}$ is the result for the 4-vertex and s -channel diagrams, $(\sigma v_{\text{lab}})_{t,u}$ is for the t - and u -channels, and $(\sigma v_{\text{lab}})_{\text{int}}$ is the interference between (4-vertex, s) and (t , u) channels, given by

$$(\sigma v_{\text{lab}})_{4v,s} = \left(3 + \frac{s(s - 4m_X^2)}{4m_X^4} \right) \frac{g_X^2 \sqrt{s - 4m_S^2}}{72\pi ((s - m_S^2)^2 + \Gamma_S^2 m_S^2) \sqrt{s}(s - 2m_X^2)} \times \left[(g_X(s - m_S^2) - g_{SSS}m_X)^2 + \Gamma_S^2 g_X^2 m_S^2 \right], \quad (\text{D2})$$

$$(\sigma v_{\text{lab}})_{t,u} = \frac{g_X^4 \sqrt{s - 4m_S^2}}{288\pi m_X^4 \sqrt{s}(s - 2m_X^2)} \times \left[4m_S^4 + 4sm_S^2 + s^2 + \frac{2(m_S^8 - 8m_X^2 m_S^6 + 24m_X^4 m_S^4 - 32m_X^6 m_S^2 + 48m_X^8)}{m_S^4 - 4m_X^2 m_S^2 + m_X^2 s} \right. \\ \left. - \frac{4(3m_S^8 - 8m_X^2 m_S^6 + (4m_X^2 m_S^2 - m_S^4)(8m_X^4 + s^2) - 2m_X^2(24m_X^6 - 2s^2 m_X^2 + s^3))}{(s - 2m_S^2)\sqrt{s - 4m_S^2}\sqrt{s - 4m_X^2}} \right. \\ \left. \times \ln \left(\frac{s - 2m_S^2 + \sqrt{s - 4m_S^2}\sqrt{s - 4m_X^2}}{s - 2m_S^2 - \sqrt{s - 4m_S^2}\sqrt{s - 4m_X^2}} \right) \right], \quad (\text{D3})$$

$$(\sigma v_{\text{lab}})_{\text{int}} = g_X^3 \frac{g_X ((s - m_S^2)^2 + \Gamma_S^2 m_S^2) - g_{SSS}m_X(s - m_S^2)}{144\pi m_X^4 ((s - m_S^2)^2 + \Gamma_S^2 m_S^2) (s - 2m_X^2) \sqrt{s}\sqrt{s - 4m_X^2}} \times \left[\sqrt{s - 4m_S^2}\sqrt{s - 4m_X^2}(s(6m_X^2 - s) - 2(2m_X^2 + s)m_S^2) \right. \\ \left. - 2((2m_X^2 + s)m_S^4 - 4m_X^2(2m_X^2 + s)m_S^2 + 2m_X^2(12m_X^4 - 2sm_X^2 + s^2)) \right. \\ \left. \times \ln \left(\frac{s - 2m_S^2 + \sqrt{s - 4m_S^2}\sqrt{s - 4m_X^2}}{s - 2m_S^2 - \sqrt{s - 4m_S^2}\sqrt{s - 4m_X^2}} \right) \right], \quad (\text{D4})$$

with s being the invariant mass of the DM pair, v_{lab} being the dark matter relative velocity in the rest frame of one of the incoming particles, and the effective coupling $g_{SSS} \equiv v\lambda_{SSS} \simeq -3g_X m_S^2/m_X$. The thermally averaged annihilation cross section $\langle \sigma v_{\text{Mol}} \rangle$ is equivalent to $\langle \sigma v_{\text{lab}} \rangle$ [71], and can be approximated as [35]

$$\langle \sigma v_{\text{Mol}} \rangle \simeq \frac{2x^{3/2}}{\sqrt{\pi}} \int_0^\infty \sigma v_{\text{lab}} \frac{(1 + 2\epsilon)\epsilon^{1/2}}{(1 + \epsilon)^{1/4}} \left(1 - \frac{15}{4x} + \frac{3}{16x(1 + \epsilon)^{1/2}} \right) e^{-\frac{x\epsilon}{(1 + \sqrt{1 + \epsilon})/2}} d\epsilon, \quad (\text{D5})$$

provided that $x(\equiv m_X/T) \gg 1$, where $\epsilon = (s - 4m_X^2)/(4m_X^2)$. For the indirect searches, assuming that the dark matter particles are locally in thermal equilibrium, we have $x^{-1} = v_p^2/(2c^2)$, with v_p the most probable speed of the DM distribution. The value of v_p/c is about $\mathcal{O}(10^{-5})$ in the dwarf spheroidal satellite galaxies [88–92] and $\mathcal{O}(10^{-3})$ in our Galactic center [93, 94]. In the low-velocity

limit, we can have $\langle \sigma v_{M\phi 1} \rangle \cong (\sigma v_{\text{lab}})_{\text{LV}}$ by taking $s \rightarrow 4m_X^2$,

$$\begin{aligned}
(\sigma v_{\text{lab}})_{\text{LV}} &= \frac{g_X^2 \sqrt{m_X^2 - m_S^2}}{144\pi m_X^3 (2m_X^2 - m_S^2)^2 ((4m_X^2 - m_S^2)^2 + \Gamma_S^2 m_S^2)} \\
&\times \left[g_X^2 ((4m_X^2 - m_S^2)^2 + \Gamma_S^2 m_S^2) (11m_S^4 - 28m_X^2 m_S^2 + 44m_X^4) \right. \\
&\left. + 3g_{SSS}^2 m_X^2 (2m_X^2 - m_S^2)^2 - 2g_{SSS} g_X m_X (m_S^6 - 16m_X^2 m_S^4 + 68m_X^4 m_S^2 - 80m_X^6) \right].
\end{aligned} \tag{D6}$$

2. The annihilation processes, $SS \rightarrow AA$ and $AA \rightarrow \tau^+ \tau^-$

In the derivation of the coupled Boltzmann equations, given in Eqs. (50) and (51), one needs to take into account the chemical equilibrium among the relevant particles. The chemical equilibrium between the CP-even scalar S and CP-odd scalar A particles depends on the magnitudes of the decay width for $S \rightarrow AA$ and annihilation cross section for $SS \rightarrow AA$. The former is described in Eqs. (23)-(26), and the latter is given by

$$\begin{aligned}
(\sigma v_{\text{lab}})_{SS \rightarrow AA} &= \frac{\sqrt{s - 4m_A^2}}{32\pi \sqrt{s} (s - 2m_S^2) ((s - m_S^2)^2 + \Gamma_S^2 m_S^2)} \\
&\times \left[g_{SAA}^2 g_{SSS}^2 - 2g_{SSAA} g_{SAA} g_{SSS} (s - m_S^2) + \lambda_{SSAA}^2 ((s - m_S^2)^2 + \Gamma_S^2 m_S^2) \right. \\
&+ \frac{2g_{SAA}^4 ((s - m_S^2)^2 + \Gamma_S^2 m_S^2)}{m_S^4 + m_A^2 (s - 4m_S^2)} \\
&- \frac{8g_{SAA}^2 \coth^{-1} \left(\frac{2m_S^2 - s}{\sqrt{s - 4m_A^2} \sqrt{s - 4m_S^2}} \right)}{\sqrt{s - 4m_A^2} \sqrt{s - 4m_S^2} (s - 2m_S^2)} \left(\Gamma_S^2 m_S^2 (g_{SAA}^2 + \lambda_{SSAA} (s - 2m_S^2)) \right. \\
&\left. \left. - (s - m_S^2) (g_{SAA} g_{SSS} (s - 2m_S^2) - g_{SAA}^2 (s - m_S^2) - \lambda_{SSAA} (2m_S^4 - 3sm_S^2 + s^2)) \right) \right],
\end{aligned} \tag{D7}$$

with $g_{SAA} \equiv v\lambda_{SAA}$ and $g_{SSS} \equiv v\lambda_{SSS}$.

The chemical equilibrium between A and τ depends on the magnitudes of the $A \rightarrow \tau^+ \tau^-$ decay width and $AA \rightarrow \tau^+ \tau^-$ annihilation cross section, for which the former is described in Eqs. (27)

and (28), and the latter is given by

$$\begin{aligned}
(\sigma v_{\text{lab}})_{AA \rightarrow \tau\tau} &= \frac{\sqrt{s - 4m_\tau^2}}{8\pi\sqrt{s}(s - 2m_A^2)} \\
&\times \left[\frac{2\bar{g}_{A\tau\tau}^4 (2m_A^4 - 4(2m_\tau^2 + s)m_A^2 + s(4m_\tau^2 + s))}{(s - 2m_A^2)\sqrt{s - 4m_A^2}\sqrt{s - 4m_\tau^2}} \ln \left(\frac{s - 2m_A^2 + \sqrt{s - 4m_A^2}\sqrt{s - 4m_\tau^2}}{s - 2m_A^2 - \sqrt{s - 4m_A^2}\sqrt{s - 4m_\tau^2}} \right) \right. \\
&\quad \left. - \frac{2\bar{g}_{A\tau\tau}^4 (m_A^4 - 4m_\tau^2 m_A^2 + 8m_\tau^4)}{m_A^4 - 4m_\tau^2 m_A^2 + m_\tau^2 s} + \frac{g_{SAA}^2 \bar{g}_{S\tau\tau}^2 s}{(s - m_S^2)^2 + \Gamma_S^2 m_S^2} \right], \tag{D8}
\end{aligned}$$

where $\bar{g}_{A\tau\tau} \equiv (m_\tau/v)g_{A\tau\tau}$ and $\bar{g}_{S\tau\tau} \equiv (m_\tau/v)g_{S\tau\tau}$ with $g_{A\tau\tau} = t_\beta$ and $g_{S\tau\tau} = (-c_\alpha s_\theta + s_\alpha s_\delta)/c_\beta$, as shown in Table I.

Appendix E: The muon $g - 2$ and constraints from τ decays and lepton universality

1. The muon $g - 2$

The contributions to a_μ in the present type-X N2HDM are approximately by the following one- and two-loop results. The one-loop contributions are given by [95]

$$\Delta a_\mu^{(1)} = \frac{m_\mu^2}{8\pi^2 v^2} \sum_{j=S,h,H,A,H^\pm} g_j^2 \frac{m_\mu^2}{m_j^2} f_j \left(\frac{m_\mu^2}{m_j^2} \right), \tag{E1}$$

with $g_{H^\pm} \equiv \tan \beta$, $g_j \equiv g_{j\mu\mu}$ for S, H and A being the normalized Yukawa couplings given in Table I, and

$$f_S(r) = f_h(r) = f_H(r) \simeq -\ln r - 7/6, \quad f_A(r) \simeq \ln r + 11/6, \quad f_{H^\pm}(r) \simeq -1/6.$$

The two-loop contributions $\Delta a_\mu^{(2)} = \Delta a_\mu^{(2-1)} + \Delta a_\mu^{(2-2)}$ are from the Barr-Zee diagrams [82, 96] with a fermion in the loop, given by

$$\Delta a_\mu^{(2-1)} = \frac{m_\mu^2}{8\pi^2 v^2} \frac{\alpha_{em}}{\pi} \sum_{\substack{j=S,h,H,A \\ f=\text{quark, lepton}}} N_c^f Q_f^2 g_{j\mu\mu} g_{jff} \frac{m_f^2}{m_j^2} g_j \left(\frac{m_f^2}{m_j^2} \right), \tag{E2}$$

and with the charged Higgs in the loop, given by

$$\Delta a_\mu^{(2-2)} = \frac{m_\mu^2}{16\pi^2} \frac{\alpha_{em}}{\pi} \sum_{j=S,h,H} g_{j\mu\mu} \lambda_{jH^+H^-} \frac{1}{m_j^2} g_j \left(\frac{m_{H^\pm}^2}{m_j^2} \right), \tag{E3}$$

where $N_c^f \equiv 3$ (1) for quarks (leptons), Q_f the electric charge of the fermion in the loop, and

$$g_i(r) = \int_0^1 \frac{N_i(x)}{x(1-x) - r} \ln \frac{x(1-x)}{r}, \tag{E4}$$

with $N_h(x) = N_H(x) \equiv 2x(1-x) - 1$, $N_A(x) \equiv 1$, and $N_{H^\pm} \equiv x(1-x)$. Here the triple Higgs couplings $\lambda_{jH^+H^-}$ equal to λ_{jAA} with m_A replaced by m_{H^\pm} ; see Eqs. (15), (16), and (17) for references.

2. Constraints from τ decays and lepton universality

The ratio of the pure leptonic processes can be parametrized as $\Gamma(\ell_1 \rightarrow \nu_1 \ell_2 \bar{\nu}_{\ell_2})/\Gamma(\ell_3 \rightarrow \nu_3 \ell_4 \bar{\nu}_{\ell_4}) \equiv (g_{\ell_1} g_{\ell_2})^2/(g_{\ell_3} g_{\ell_4})^2$. In the present model, three parameters for the $\delta_{\ell\ell'} (\equiv (g_{\ell}/g_{\ell'}) - 1)$, which describe the deviations from the SM results, can be obtained from the data, $\tau \rightarrow \mu\nu\bar{\nu}$, $\tau \rightarrow e\nu\bar{\nu}$ and $\mu \rightarrow e\nu\bar{\nu}$ [97], and are given by

$$\delta_{\tau\mu} = \delta_{\text{loop}}, \quad \delta_{\tau e} = \delta_{\text{tree}} + \delta_{\text{loop}}, \quad \delta_{\mu e} = \delta_{\text{tree}}, \quad (\text{E5})$$

where the theoretical formulas for δ_{tree} and δ_{loop} are [98]

$$\begin{aligned} \delta_{\text{tree}} &= \frac{m_\tau^2 m_\mu^2}{8m_{H^\pm}^4} t_\beta^4 - \frac{m_\mu^2}{m_{H^\pm}^2} t_\beta^2 \frac{g(m_\mu^2/m_\tau^2)}{f(m_\mu^2/m_\tau^2)}, \\ \delta_{\text{loop}} &= \frac{G_F m_\tau^2}{8\sqrt{2}\pi^2} t_\beta^2 \left[1 + \frac{1}{4} \left(H(x_A) + s_{\beta-\alpha}^2 H(x_H) + c_{\beta-\alpha}^2 H(x_h) + (s_{\beta-\alpha} s_\theta + c_{\beta-\alpha} s_\delta)^2 H(x_S) \right) \right], \end{aligned} \quad (\text{E6})$$

with $g(x) \equiv 1 + 9x - 9x^2 - x^3 + 6x(1+x)\ln x$, $f(x) \equiv 1 - 8x + 8x^3 - x^4 - 12x^2 \ln x$, $H(x) \equiv (\ln x)(1+x)/(1-x)$, and $x_\phi = m_\phi^2/m_{H^\pm}^2$. Further considering the data of the semi-hadronic processes $\pi/K \rightarrow \mu\nu$ that can also give the value of $\delta_{\tau\mu}$ [97], Chun, Kang, Takeuchi, and Tsai [99] obtained the following three independent constraints,

$$\begin{aligned} \frac{1}{\sqrt{2}}\delta_{\text{tree}} + \sqrt{2}\delta_{\text{loop}} &= 0.0028 \pm 0.0019, \\ \sqrt{\frac{3}{2}}\delta_{\text{tree}} &= 0.0022 \pm 0.0017, \\ \delta_{\text{loop}} &= 0.0001 \pm 0.0014. \end{aligned} \quad (\text{E7})$$

We use the above results to show the constraint on the m_A - $\tan\beta$ plane in Fig. 10.

-
- [1] L. Goodenough and D. Hooper, ‘‘Possible Evidence For Dark Matter Annihilation In The Inner Milky Way From The Fermi Gamma Ray Space Telescope,’’ arXiv:0910.2998 [hep-ph].
 - [2] D. Hooper and L. Goodenough, ‘‘Dark Matter Annihilation in The Galactic Center As Seen by the Fermi Gamma Ray Space Telescope,’’ Phys. Lett. B **697**, 412 (2011) [arXiv:1010.2752 [hep-ph]].
 - [3] D. Hooper and T. Linden, ‘‘On The Origin Of The Gamma Rays From The Galactic Center,’’ Phys. Rev. D **84**, 123005 (2011) [arXiv:1110.0006 [astro-ph.HE]].
 - [4] K. N. Abazajian and M. Kaplinghat, ‘‘Detection of a Gamma-Ray Source in the Galactic Center Consistent with Extended Emission from Dark Matter Annihilation and Concentrated Astrophysical Emission,’’ Phys. Rev. D **86**, 083511 (2012) Erratum: [Phys. Rev. D **87**, 129902 (2013)] [arXiv:1207.6047 [astro-ph.HE]].

- [5] C. Gordon and O. Macias, “Dark Matter and Pulsar Model Constraints from Galactic Center Fermi-LAT Gamma Ray Observations,” *Phys. Rev. D* **88**, no. 8, 083521 (2013) Erratum: [*Phys. Rev. D* **89**, no. 4, 049901 (2014)] [arXiv:1306.5725 [astro-ph.HE]].
- [6] W. C. Huang, A. Urbano and W. Xue, “Fermi Bubbles under Dark Matter Scrutiny. Part I: Astrophysical Analysis,” arXiv:1307.6862 [hep-ph].
- [7] T. Daylan, D. P. Finkbeiner, D. Hooper, T. Linden, S. K. N. Portillo, N. L. Rodd and T. R. Slatyer, “The characterization of the gamma-ray signal from the central Milky Way: A case for annihilating dark matter,” *Phys. Dark Univ.* **12**, 1 (2016) [arXiv:1402.6703 [astro-ph.HE]].
- [8] F. Calore, I. Cholis and C. Weniger, “Background model systematics for the Fermi GeV excess,” *JCAP* **1503**, 038 (2015) [arXiv:1409.0042 [astro-ph.CO]].
- [9] F. Calore, I. Cholis, C. McCabe and C. Weniger, “A Tale of Tails: Dark Matter Interpretations of the Fermi GeV Excess in Light of Background Model Systematics,” *Phys. Rev. D* **91**, no. 6, 063003 (2015) [arXiv:1411.4647 [hep-ph]].
- [10] C. Karwin, S. Murgia, T. M. P. Tait, T. A. Porter and P. Tanedo, “Dark Matter Interpretation of the Fermi-LAT Observation Toward the Galactic Center,” *Phys. Rev. D* **95**, no. 10, 103005 (2017) [arXiv:1612.05687 [hep-ph]].
- [11] M. Ackermann *et al.* [Fermi-LAT Collaboration], “The Fermi Galactic Center GeV Excess and Implications for Dark Matter,” *Astrophys. J.* **840**, no. 1, 43 (2017) [arXiv:1704.03910 [astro-ph.HE]].
- [12] R. M. O’Leary, M. D. Kistler, M. Kerr and J. Dexter, “Young and Millisecond Pulsar GeV Gamma-ray Fluxes from the Galactic Center and Beyond,” arXiv:1601.05797 [astro-ph.HE].
- [13] M. Ajello *et al.* [Fermi-LAT Collaboration], “Characterizing the population of pulsars in the Galactic bulge with the *Fermi* Large Area Telescope,” [arXiv:1705.00009 [astro-ph.HE]].
- [14] H. Ploeg, C. Gordon, R. Crocker and O. Macias, “Consistency Between the Luminosity Function of Resolved Millisecond Pulsars and the Galactic Center Excess,” *JCAP* **1708**, no. 08, 015 (2017) [arXiv:1705.00806 [astro-ph.HE]].
- [15] D. Hooper and G. Mohlabeng, “The Gamma-Ray Luminosity Function of Millisecond Pulsars and Implications for the GeV Excess,” *JCAP* **1603**, no. 03, 049 (2016) [arXiv:1512.04966 [astro-ph.HE]].
- [16] I. Cholis, C. Evoli, F. Calore, T. Linden, C. Weniger and D. Hooper, “The Galactic Center GeV Excess from a Series of Leptonic Cosmic-Ray Outbursts,” *JCAP* **1512**, no. 12, 005 (2015) [arXiv:1506.05119 [astro-ph.HE]].
- [17] J. Petrović, P. D. Serpico and G. Zaharijas, “Galactic Center gamma-ray ”excess” from an active past of the Galactic Centre?,” *JCAP* **1410**, no. 10, 052 (2014) [arXiv:1405.7928 [astro-ph.HE]].
- [18] E. Carlson and S. Profumo, “Cosmic Ray Protons in the Inner Galaxy and the Galactic Center Gamma-Ray Excess,” *Phys. Rev. D* **90**, no. 2, 023015 (2014) [arXiv:1405.7685 [astro-ph.HE]].
- [19] C. Boehm, M. J. Dolan, C. McCabe, M. Spannowsky and C. J. Wallace, “Extended gamma-ray emission from Coy Dark Matter,” *JCAP* **1405**, 009 (2014) [arXiv:1401.6458 [hep-ph]].

- [20] A. Hektor and L. Marzola, “Coy Dark Matter and the anomalous magnetic moment,” *Phys. Rev. D* **90**, no. 5, 053007 (2014) [arXiv:1403.3401 [hep-ph]].
- [21] C. Arina, E. Del Nobile and P. Panci, “Dark Matter with Pseudoscalar-Mediated Interactions Explains the DAMA Signal and the Galactic Center Excess,” *Phys. Rev. Lett.* **114**, 011301 (2015) [arXiv:1406.5542 [hep-ph]].
- [22] A. Hektor, K. Kannike and L. Marzola, “Muon $g - 2$ and Galactic Centre gamma-ray excess in a scalar extension of the 2HDM type-X,” *JCAP* **1510**, no. 10, 025 (2015) [arXiv:1507.05096 [hep-ph]].
- [23] O. Lebedev, H. M. Lee and Y. Mambrini, “Vector Higgs-portal dark matter and the invisible Higgs,” *Phys. Lett. B* **707**, 570 (2012) [arXiv:1111.4482 [hep-ph]].
- [24] Y. Farzan and A. R. Akbarieh, “VDM: A model for Vector Dark Matter,” *JCAP* **1210**, 026 (2012) [arXiv:1207.4272 [hep-ph]].
- [25] S. Baek, P. Ko, W. I. Park and E. Senaha, “Higgs Portal Vector Dark Matter : Revisited,” *JHEP* **1305**, 036 (2013) [arXiv:1212.2131 [hep-ph]].
- [26] S. Baek, P. Ko, W. I. Park and Y. Tang, “Indirect and direct signatures of Higgs portal decaying vector dark matter for positron excess in cosmic rays,” *JCAP* **1406**, 046 (2014) [arXiv:1402.2115 [hep-ph]].
- [27] P. Ko, W. I. Park and Y. Tang, “Higgs portal vector dark matter for GeV scale γ -ray excess from galactic center,” *JCAP* **1409**, 013 (2014) [arXiv:1404.5257 [hep-ph]].
- [28] M. S. Boucenna and S. Profumo, “Direct and Indirect Singlet Scalar Dark Matter Detection in the Lepton-Specific two-Higgs-doublet Model,” *Phys. Rev. D* **84**, 055011 (2011) [arXiv:1106.3368 [hep-ph]].
- [29] M. Escudero, S. J. Witte and D. Hooper, “Hidden Sector Dark Matter and the Galactic Center Gamma-Ray Excess: A Closer Look,” *JCAP* **1711**, no. 11, 042 (2017) [arXiv:1709.07002 [hep-ph]].
- [30] P. Ko and Y. Tang, “Galactic center γ -ray excess in hidden sector DM models with dark gauge symmetries: local Z_3 symmetry as an example,” *JCAP* **1501**, 023 (2015) [arXiv:1407.5492 [hep-ph]].
- [31] M. Abdullah, A. DiFranzo, A. Rajaraman, T. M. P. Tait, P. Tanedo and A. M. Wijangco, “Hidden on-shell mediators for the Galactic Center γ -ray excess,” *Phys. Rev. D* **90**, 035004 (2014) [arXiv:1404.6528 [hep-ph]].
- [32] A. Martin, J. Shelton and J. Unwin, “Fitting the Galactic Center Gamma-Ray Excess with Cascade Annihilations,” *Phys. Rev. D* **90**, no. 10, 103513 (2014) [arXiv:1405.0272 [hep-ph]].
- [33] A. Berlin, P. Gratia, D. Hooper and S. D. McDermott, “Hidden Sector Dark Matter Models for the Galactic Center Gamma-Ray Excess,” *Phys. Rev. D* **90**, no. 1, 015032 (2014) [arXiv:1405.5204 [hep-ph]].
- [34] Y. G. Kim, K. Y. Lee, C. B. Park and S. Shin, “Secluded singlet fermionic dark matter driven by the Fermi gamma-ray excess,” *Phys. Rev. D* **93**, no. 7, 075023 (2016) [arXiv:1601.05089 [hep-ph]].
- [35] K. C. Yang, “Search for Scalar Dark Matter via Pseudoscalar Portal Interactions: In Light of the Galactic Center Gamma-Ray Excess,” *Phys. Rev. D* **97**, no. 2, 023025 (2018) [arXiv:1711.03878 [hep-ph]].

- [36] C. Boehm, M. J. Dolan and C. McCabe, “A weighty interpretation of the Galactic Centre excess,” *Phys. Rev. D* **90**, no. 2, 023531 (2014) [arXiv:1404.4977 [hep-ph]].
- [37] M. Pospelov, A. Ritz and M. B. Voloshin, “Secluded WIMP Dark Matter,” *Phys. Lett. B* **662**, 53 (2008) [arXiv:0711.4866 [hep-ph]].
- [38] J. Mardon, Y. Nomura, D. Stolarski and J. Thaler, “Dark Matter Signals from Cascade Annihilations,” *JCAP* **0905**, 016 (2009) [arXiv:0901.2926 [hep-ph]].
- [39] D. Hooper, N. Weiner and W. Xue, “Dark Forces and Light Dark Matter,” *Phys. Rev. D* **86**, 056009 (2012) [arXiv:1206.2929 [hep-ph]].
- [40] S. Profumo, F. S. Queiroz, J. Silk and C. Siqueira, “Searching for Secluded Dark Matter with H.E.S.S., Fermi-LAT, and Planck,” *JCAP* **1803**, no. 03, 010 (2018) [arXiv:1711.03133 [hep-ph]].
- [41] G. Elor, N. L. Rodd and T. R. Slatyer, “Multistep cascade annihilations of dark matter and the Galactic Center excess,” *Phys. Rev. D* **91**, 103531 (2015) [arXiv:1503.01773 [hep-ph]].
- [42] G. Elor, N. L. Rodd, T. R. Slatyer and W. Xue, “Model-Independent Indirect Detection Constraints on Hidden Sector Dark Matter,” *JCAP* **1606**, no. 06, 024 (2016) [arXiv:1511.08787 [hep-ph]].
- [43] L. Wang and X. F. Han, “A light pseudoscalar of 2HDM confronted with muon $g-2$ and experimental constraints,” *JHEP* **1505**, 039 (2015) [arXiv:1412.4874 [hep-ph]].
- [44] T. Abe, R. Sato and K. Yagyu, “Lepton-specific two Higgs doublet model as a solution of muon $g-2$ anomaly,” *JHEP* **1507**, 064 (2015) [arXiv:1504.07059 [hep-ph]].
- [45] E. J. Chun and J. Kim, “Leptonic Precision Test of Leptophilic Two-Higgs-Doublet Model,” *JHEP* **1607**, 110 (2016) [arXiv:1605.06298 [hep-ph]].
- [46] J. A. Dror, E. Kuflik and W. H. Ng, “Codecaying Dark Matter,” *Phys. Rev. Lett.* **117**, no. 21, 211801 (2016) [arXiv:1607.03110 [hep-ph]].
- [47] M. Farina, D. Pappadopulo, J. T. Ruderman and G. Trevisan, “Phases of Cannibal Dark Matter,” *JHEP* **1612**, 039 (2016) [arXiv:1607.03108 [hep-ph]].
- [48] D. Pappadopulo, J. T. Ruderman and G. Trevisan, “Dark matter freeze-out in a nonrelativistic sector,” *Phys. Rev. D* **94**, no. 3, 035005 (2016) [arXiv:1602.04219 [hep-ph]].
- [49] A. Karam and K. Tamvakis, “Dark Matter from a Classically Scale-Invariant $SU(3)_X$,” *Phys. Rev. D* **94**, no. 5, 055004 (2016) [arXiv:1607.01001 [hep-ph]].
- [50] A. Karam and K. Tamvakis, “Dark matter and neutrino masses from a scale-invariant multi-Higgs portal,” *Phys. Rev. D* **92**, no. 7, 075010 (2015) [arXiv:1508.03031 [hep-ph]].
- [51] P. M. Ferreira, J. F. Gunion, H. E. Haber and R. Santos, “Probing wrong-sign Yukawa couplings at the LHC and a future linear collider,” *Phys. Rev. D* **89**, no. 11, 115003 (2014) [arXiv:1403.4736 [hep-ph]].
- [52] G. Aad *et al.* [ATLAS and CMS Collaborations], “Combined Measurement of the Higgs Boson Mass in pp Collisions at $\sqrt{s} = 7$ and 8 TeV with the ATLAS and CMS Experiments,” *Phys. Rev. Lett.* **114**, 191803 (2015) [arXiv:1503.07589 [hep-ex]].
- [53] V. Khachatryan *et al.* [CMS Collaboration], “Search for light bosons in decays of the 125 GeV Higgs boson in proton-proton collisions at $\sqrt{s} = 8$ TeV,” *JHEP* **1710**, 076 (2017) [arXiv:1701.02032 [hep-ex]].

- [54] D. Curtin *et al.*, “Exotic decays of the 125 GeV Higgs boson,” *Phys. Rev. D* **90**, no. 7, 075004 (2014) [arXiv:1312.4992 [hep-ph]].
- [55] G. Aad *et al.* [ATLAS and CMS Collaborations], “Measurements of the Higgs boson production and decay rates and constraints on its couplings from a combined ATLAS and CMS analysis of the LHC pp collision data at $\sqrt{s} = 7$ and 8 TeV,” *JHEP* **1608**, 045 (2016) doi:10.1007/JHEP08(2016)045 [arXiv:1606.02266 [hep-ex]].
- [56] M. E. Peskin and T. Takeuchi, “Estimation of oblique electroweak corrections,” *Phys. Rev. D* **46**, 381 (1992).
- [57] M. E. Peskin and T. Takeuchi, “A New constraint on a strongly interacting Higgs sector,” *Phys. Rev. Lett.* **65**, 964 (1990).
- [58] W. Grimus, L. Lavoura, O. M. Ogreid and P. Osland, “The Oblique parameters in multi-Higgs-doublet models,” *Nucl. Phys. B* **801**, 81 (2008) [arXiv:0802.4353 [hep-ph]].
- [59] M. Cirelli *et al.*, “PPPC 4 DM ID: A Poor Particle Physicist Cookbook for Dark Matter Indirect Detection,” *JCAP* **1103**, 051 (2011) Erratum: [*JCAP* **1210**, E01 (2012)] [arXiv:1012.4515 [hep-ph]].
- [60] P. Ciafaloni, D. Comelli, A. Riotto, F. Sala, A. Strumia and A. Urbano, “Weak Corrections are Relevant for Dark Matter Indirect Detection,” *JCAP* **1103**, 019 (2011) [arXiv:1009.0224 [hep-ph]].
- [61] T. Sjostrand, S. Mrenna and P. Z. Skands, “A Brief Introduction to PYTHIA 8.1,” *Comput. Phys. Commun.* **178**, 852 (2008) [arXiv:0710.3820 [hep-ph]].
- [62] T. Linden, N. L. Rodd, B. R. Safdi and T. R. Slatyer, “High-energy tail of the Galactic Center gamma-ray excess,” *Phys. Rev. D* **94**, no. 10, 103013 (2016) [arXiv:1604.01026 [astro-ph.HE]].
- [63] J. F. Navarro, C. S. Frenk and S. D. M. White, “The Structure of cold dark matter halos,” *Astrophys. J.* **462**, 563 (1996) [astro-ph/9508025].
- [64] J. F. Navarro, C. S. Frenk and S. D. M. White, “A Universal density profile from hierarchical clustering,” *Astrophys. J.* **490**, 493 (1997) [astro-ph/9611107].
- [65] A. Albert *et al.* [Fermi-LAT and DES Collaborations], “Searching for Dark Matter Annihilation in Recently Discovered Milky Way Satellites with Fermi-LAT,” *Astrophys. J.* **834**, no. 2, 110 (2017) [arXiv:1611.03184 [astro-ph.HE]].
- [66] The data is available from the website: “http://www-glast.stanford.edu/pub_data/1203/”.
- [67] M. Ackermann *et al.* [Fermi-LAT Collaboration], “Searching for Dark Matter Annihilation from Milky Way Dwarf Spheroidal Galaxies with Six Years of Fermi Large Area Telescope Data,” *Phys. Rev. Lett.* **115**, no. 23, 231301 (2015) [arXiv:1503.02641 [astro-ph.HE]].
- [68] Maja Garde Lindholm, “PhD thesis at Stockholm University: Dark Matter searches targeting Dwarf Spheroidal Galaxies with the Fermi Large Area Telescope”, ISBN 978-91-7649-224-6, printed by Publit, Stockholm, Sweden, 2015.
- [69] B. Anderson *et al.* [Fermi-LAT Collaboration], “Using Likelihood for Combined Data Set Analysis,” arXiv:1502.03081 [astro-ph.HE].

- [70] E. Charles *et al.* [Fermi-LAT Collaboration], “Sensitivity Projections for Dark Matter Searches with the Fermi Large Area Telescope,” *Phys. Rept.* **636**, 1 (2016) [arXiv:1605.02016 [astro-ph.HE]].
- [71] P. Gondolo and G. Gelmini, “Cosmic abundances of stable particles: Improved analysis,” *Nucl. Phys. B* **360**, 145 (1991).
- [72] D. G. Cerdeno, T. Delahaye and J. Lavalle, “Cosmic-ray antiproton constraints on light singlino-like dark matter candidates,” *Nucl. Phys. B* **854**, 738 (2012) [arXiv:1108.1128 [hep-ph]].
- [73] C. Patrignani *et al.* (Particle Data Group), *Chin. Phys. C*, 40, 100001 (2016) and 2017 update.
- [74] S. Dodelson, *Modern Cosmology*. Academic Press, 2003.
- [75] A. Berlin, D. Hooper and G. Krnjaic, “Thermal Dark Matter From A Highly Decoupled Sector,” *Phys. Rev. D* **94**, no. 9, 095019 (2016) [arXiv:1609.02555 [hep-ph]].
- [76] P. A. R. Ade *et al.* [Planck Collaboration], “Planck 2013 results. XVI. Cosmological parameters,” *Astron. Astrophys.* **571**, A16 (2014) [arXiv:1303.5076 [astro-ph.CO]].
- [77] M. Kawasaki, K. Kohri and N. Sugiyama, “MeV scale reheating temperature and thermalization of neutrino background,” *Phys. Rev. D* **62**, 023506 (2000) [astro-ph/0002127].
- [78] P. A. R. Ade *et al.* [Planck Collaboration], “Planck 2015 results. XIII. Cosmological parameters,” *Astron. Astrophys.* **594**, A13 (2016) [arXiv:1502.01589 [astro-ph.CO]].
- [79] G. W. Bennett *et al.* [Muon g-2 Collaboration], “Final Report of the Muon E821 Anomalous Magnetic Moment Measurement at BNL,” *Phys. Rev. D* **73**, 072003 (2006) [hep-ex/0602035].
- [80] A. Broggio, E. J. Chun, M. Passera, K. M. Patel and S. K. Vempati, “Limiting two-Higgs-doublet models,” *JHEP* **1411**, 058 (2014) [arXiv:1409.3199 [hep-ph]].
- [81] M. Davier, A. Hoecker, B. Malaescu and Z. Zhang, “Reevaluation of the Hadronic Contributions to the Muon g-2 and to $\alpha(M_Z)$,” *Eur. Phys. J. C* **71**, 1515 (2011) Erratum: [*Eur. Phys. J. C* **72**, 1874 (2012)] [arXiv:1010.4180 [hep-ph]].
- [82] K. m. Cheung, C. H. Chou and O. C. W. Kong, “Muon anomalous magnetic moment, two Higgs doublet model, and supersymmetry,” *Phys. Rev. D* **64** (2001) 111301 [hep-ph/0103183].
- [83] J. Wittbrodt, Master Thesis, 2016, Karlsruhe Institute of Technology (2016).
- [84] M. Muhlleitner, M. O. P. Sampaio, R. Santos and J. Wittbrodt, “The N2HDM under Theoretical and Experimental Scrutiny,” *JHEP* **1703**, 094 (2017) [arXiv:1612.01309 [hep-ph]].
- [85] M. Krause, D. Lopez-Val, M. Muhlleitner and R. Santos, “Gauge-independent Renormalization of the N2HDM,” arXiv:1708.01578 [hep-ph].
- [86] I. Maksymyk, C. P. Burgess and D. London, “Beyond S, T and U,” *Phys. Rev. D* **50**, 529 (1994) [hep-ph/9306267].
- [87] A. Kundu and P. Roy, “A General treatment of oblique parameters,” *Int. J. Mod. Phys. A* **12**, 1511 (1997) [hep-ph/9603323].
- [88] M. G. Walker, M. Mateo, E. W. Olszewski, O. Y. Gnedin, X. Wang, B. Sen and M. Woodroffe, “Velocity Dispersion Profiles of Seven Dwarf Spheroidal Galaxies,” *Astrophys. J.* **667**, L53 (2007) [arXiv:0708.0010 [astro-ph]].

- [89] N. F. Martin, J. T. A. de Jong and H. W. Rix, “A comprehensive Maximum Likelihood analysis of the structural properties of faint Milky Way satellites,” *Astrophys. J.* **684**, 1075 (2008) [arXiv:0805.2945 [astro-ph]].
- [90] M. Geha, B. Willman, J. D. Simon, L. E. Strigari, E. N. Kirby, D. R. Law and J. Strader, “The Least Luminous Galaxy: Spectroscopy of the Milky Way Satellite Segue 1,” *Astrophys. J.* **692**, 1464 (2009) [arXiv:0809.2781 [astro-ph]].
- [91] M. G. Walker, M. Mateo, E. W. Olszewski, J. Penarrubia, N. W. Evans and G. Gilmore, “A Universal Mass Profile for Dwarf Spheroidal Galaxies,” *Astrophys. J.* **704**, 1274 (2009) Erratum: [*Astrophys. J.* **710**, 886 (2010)] [arXiv:0906.0341 [astro-ph.CO]].
- [92] J. D. Simon and M. Geha, “The Kinematics of the Ultra-Faint Milky Way Satellites: Solving the Missing Satellite Problem,” *Astrophys. J.* **670**, 313 (2007) [arXiv:0706.0516 [astro-ph]].
- [93] G. Battaglia *et al.*, “The Radial velocity dispersion profile of the Galactic Halo: Constraining the density profile of the dark halo of the Milky Way,” *Mon. Not. Roy. Astron. Soc.* **364**, 433 (2005) Erratum: [*Mon. Not. Roy. Astron. Soc.* **370**, 1055 (2006)] [astro-ph/0506102].
- [94] W. Dehnen, D. McLaughlin and J. Sachania, “The velocity dispersion and mass profile of the milky way,” *Mon. Not. Roy. Astron. Soc.* **369**, 1688 (2006) [astro-ph/0603825].
- [95] A. Dedes and H. E. Haber, “Can the Higgs sector contribute significantly to the muon anomalous magnetic moment?,” *JHEP* **0105**, 006 (2001) [hep-ph/0102297].
- [96] V. Ilisie, “New Barr-Zee contributions to $(\mathbf{g} - \mathbf{2})_\mu$ in two-Higgs-doublet models,” *JHEP* **1504**, 077 (2015) [arXiv:1502.04199 [hep-ph]].
- [97] Y. Amhis *et al.* [Heavy Flavor Averaging Group (HFAG)], “Averages of b -hadron, c -hadron, and τ -lepton properties as of summer 2014,” arXiv:1412.7515 [hep-ex].
- [98] M. Krawczyk and D. Temes, “2HDM(II) radiative corrections in leptonic tau decays,” *Eur. Phys. J. C* **44**, 435 (2005) [hep-ph/0410248].
- [99] E. J. Chun, Z. Kang, M. Takeuchi and Y. L. S. Tsai, “LHC τ -rich tests of lepton-specific 2HDM for $(\mathbf{g}-2)_\mu$,” *JHEP* **1511**, 099 (2015) [arXiv:1507.08067 [hep-ph]].